ACS OMEGA

Article

Cite This: ACS Omega 2019, 4, 12955−12968

http://pubs.acs.org/journal/acsodf

Antibody−Drug Conjugate that Exhibits Synergistic Cytotoxicity with an Endosome−Disruptive Peptide

Kelsey E. Knewtson, Chamani Perera, David Hymel,[‡] Zhe Gao,[†] Molly M. Lee,[§] and Blake R. Peterson*

Department of Medicinal Chemistry, The University of Kansas, Lawrence, Kansas 66045, United States

Supporting Information

ABSTRACT: Antibody−drug conjugates are an important class of cancer therapeutics. These agents generally bind a specific cell surface receptor, undergo receptor-mediated endocytosis, and enter the endosomal−lysosomal system, where the environment in these organelles facilitates the release of a membrane-permeable cytotoxin. By using a membrane-impermeable cytotoxin, we describe here a method that allows the cytotoxicity of an antibody conjugate to be triggered by co-administration with an endosome-disruptive peptide that exhibits low toxicity. This approach was validated by conjugation of an anionic derivative of the tubulin-binding cytotoxin colchinol methyl ether to lysine residues of the HER2-targeting antibody trastuzumab (Herceptin) via a disulfide. When this antibody binds HER2 on SKBR3 breast cancer cells and undergoes endocytosis, the membrane-impermeable cytotoxin is released, but it becomes trapped in endosomes, resulting in relatively low cytotoxicity (IC_{50} > 1 μM). However, co-administration with an essentially nontoxic (IC_{50} > 10 μM) cholesterol-linked endosome-disruptive peptide promotes the release of this small molecule into the cytoplasm, conferring subnanomolar cytotoxic potency (IC_{50} = 0.11 ± 0.07 nM). Studies of a structurally related fluorophore conjugate revealed that the endosome-disruptive peptide does not substantially enhance cleavage of the disulfide ($t_{1/2}$ = 8 ± 2 h) within endosomes, suggesting that the mechanism of endosomal escape involves the efflux of some small molecules without facilitating substantial influx of reduced glutathione.

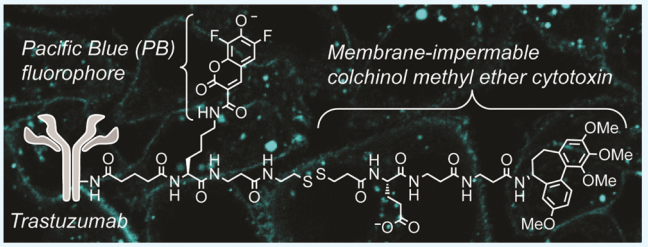

INTRODUCTION

Antibody−drug conjugates (ADCs) are under extensive development as targeted therapeutics.[1] The approval by the FDA and EMA of Adcetris (brentuximab vedotin, targeting CD30 in Hodgkin lymphoma)[2] and Kadcyla (ado-trastuzumab emtansine, targeting HER2 in breast cancer)[3] has catalyzed numerous basic and clinical studies of a wide range of next-generation conjugates, with particular emphasis on oncology.[1] Most antibody−cytotoxin conjugates bind internalizing cell surface receptors that cycle between the plasma membrane and endosomes, providing a mechanism for delivery of agents into these acidic intracellular compartments. The dissociation from receptors in endosomes and fusion of endosomes with lysosomes exposes these conjugates to more highly hydrolytic and acidic environments where proteases and other enzymes can facilitate cleavage of linkers between the protein and cytotoxin. Liberated small molecules generally diffuse across membranes of endosomes or lysosomes and manifest cytotoxicity by engaging targets in the cytoplasm or nucleus of cells.

Effective ADCs must exhibit sufficient stability to reach targeted cells but also be labile enough to release small-molecule cargo at the target site. To attain this profile, a variety of linker structures, including acid-labile hydrazones,[4−6] noncleavable thioethers that require extensive antibody proteolysis for release,[7−10] specific protease substrates,[11−13] and disulfides,[14−17] have been investigated. However, variations in the rates of cleavage of these linkers in different cell types may affect efficacy and off-target toxicity. Additionally, ADCs may exhibit undesired toxicity by binding cognate antigens on nontarget cells, through uptake by nontarget cells that express Fc receptors, or via premature release of toxins that diffuse from targeted cells into neighboring cells.[18] This premature release is of greatest concern when the toxin is highly cell-permeable. In contrast, less cell-permeable toxins may exhibit fewer side effects,[19−21] but restricting the ability to cross membranes can also reduce engagement of intracellular targets responsible for cytotoxicity. To better control the activities of ADCs, chemical strategies for triggering the release of drugs from antibodies are under investigation.[22,23]

One approach that has been used to promote the release of cargo into the cytoplasm of mammalian cells involves the disruption of intracellular endosomes. Both natural and synthetic agents have been used to promote the escape of entrapped molecules from these membrane-sealed compartments.[24−26] This approach has been used for the delivery of nucleic acids,[27,28] fluorophores,[29,30] and targeted immunotoxins[31] into the cytosol. We previously reported[32] the synthesis

Received: June 17, 2019
Accepted: July 17, 2019
Published: July 31, 2019

DOI: 10.1021/acsomega.9b01585
ACS Omega 2019, 4, 12955−12968

of a cholesterylamine-linked peptide that selectively disrupts membranes of early and recycling endosomes. This peptide was used to release a disulfide derivative of fluorescein, delivered into endosomes by conjugation to a cholesteryl-amine, into the cytoplasm and nucleus. Here, we describe the use of this approach to release cell-impermeable small molecules from endosomes delivered as conjugates of the antibody trastuzumab (Herceptin). Trastuzumab was particularly attractive for this strategy because when this anticancer antibody binds its target protein HER2 on the surface of breast cancer cells, it rapidly undergoes receptor-mediated endocytosis, but upon delivery to early/recycling endosomes, it is predominantly recycled back to the cell surface, and only a small fraction traffics to the lysosome.[33] Some other anticancer antibodies such as rituximab[34] are less likely to synergize with endosome-disruptive peptides because they are not rapidly internalized upon binding cognate cell surface antigens. As shown in Figure 1, we reasoned that the cytotoxicity of an

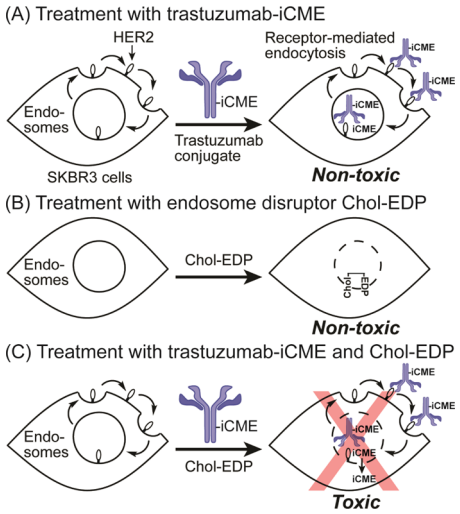

Figure 1. Strategy for activation of an antibody−cytotoxin conjugate (trastuzumab−iCME) by an endosome-disruptive peptide (Chol-EDP). Trastuzumab−iCME alone was designed to be essentially nontoxic (panel A) as a result of low membrane permeability of the linked colchinol methyl ether derivative (iCME). Chol-EDP was designed to similarly exhibit low toxicity (panel B). In combination, Chol-EDP triggers the release of the iCME warhead into the cytoplasm (panel C), resulting in toxicity.

impermeable cytotoxin warhead delivered as a trastuzumab conjugate might be triggered by an endosome-disruptive peptide, limiting the effects of the cytotoxin on nontargeted cells. Using a cell-impermeable derivative of the cytotoxin colchinol methyl ether (iCME) linked to trastuzumab and an optimized cholesterol-linked endosome-disruptive peptide (Chol-EDP), we demonstrate that these two agents show low cytotoxicity individually, but when combined, potently kill HER2-positive SKBR3 cells, while sparing HER2-negative MDA-MB-468 cells.

RESULTS AND DISCUSSION

Design and Synthesis. To validate the concept that a small molecule delivered by an antibody can be released by co-administration with an endosome-disruptive lipopeptide, we designed fluorescein disulfide conjugates of the HER2-targeted antibody trastuzumab (**1**) and human IgG (**2**) as a nontargeted control (Figure 2). We additionally designed a novel endosome-disruptive peptide termed here Chol-EDP (**3**,

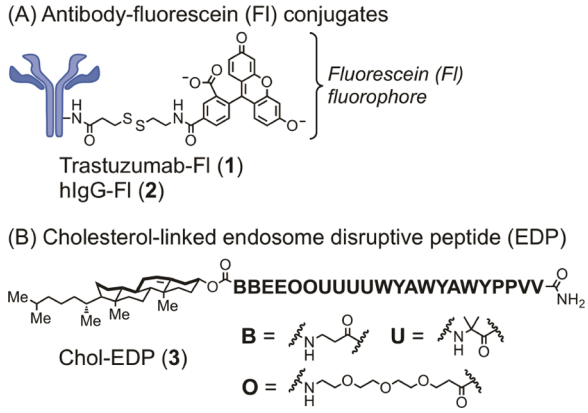

Figure 2. Structures of disulfide-linked antibody−fluorescein conjugates (**1**, **2**, panel A) and a novel cholesterol-linked endosome-disruptive peptide (**3**, panel B). In panel B, letters in bold either represent natural L-amino acids or are defined as specific non-proteogenic amino acids.

Figure 2) that is structurally related to our previously reported[32] cholesterylamine-modified PC4 peptide.[35] Chol-EDP (**3**) differs from cholesterylamine-PC4 in its cholesteryl carbamate membrane anchor, the incorporation of solubility-enhancing ethylene glycol-containing amino acids (O), and conformationally constraining Aib (U) residues known to promote helix formation,[36] and it adds three additional amino acids in the aromatic-rich region to better complement the 36−43 Å thickness[37] of membranes of mammalian cells. The comparison of the structures of these peptides is shown in the Supporting Information (Figure S1).

We further designed targeted trastuzumab and nontargeted hIgG antibody conjugates (**4**, **5**) bearing an anionic (poorly cell permeable) derivative of the tubulin-binding cytotoxin colchinol methyl ether (iCME, Figure 3). These lysine conjugates include a linker containing β-alanines, a glutamic acid residue to limit cell permeability of the small molecule, a disulfide amino acid, and a lysine modified with Pacific Blue (PB),[38] a fluorescent probe that was used for both detection and quantification of the degree of antibody labeling (DOL). Colchinol methyl ether (CME) is an analogue of the plant natural product colchicine. This natural product inhibits mitosis by binding tubulin,[39] and it has been previously investigated[40,41] linked to tumor-targeted cytotoxins. In CME, the tropone ring of colchicine is contracted to form a benzene. This modification increases potency for inhibition of tubulin and decreases off-target effects.[42,43] A trastuzumab conjugate that substitutes CME with the comparably hydrophobic Pennsylvania Green (PG)[44,45] fluorophore (**6**) was designed as a structurally related mechanistic probe. Analogues of CME designed to be cell-permeable (**7**) and cell-impermeable (**8**) were designed as positive (**7**) and negative (**8**) control compounds.

Synthesis of the 5-carboxyfluorescein-disulfide-NHS ester used to prepare antibody conjugates **1** and **2** is described in the Experimental Section. The synthesis of more complex NHS esters used to generate antibody conjugates **4**−**6** is shown in Figure 4. Deacetylcolchinol methyl ether (**11**) was synthesized as previously reported.[46,47] Antibody conjugates **1**, **2** and **4**−**6** were prepared by random modification of lysine residues with

DOI: 10.1021/acsomega.9b01585
ACS Omega 2019, 4, 12955−12968

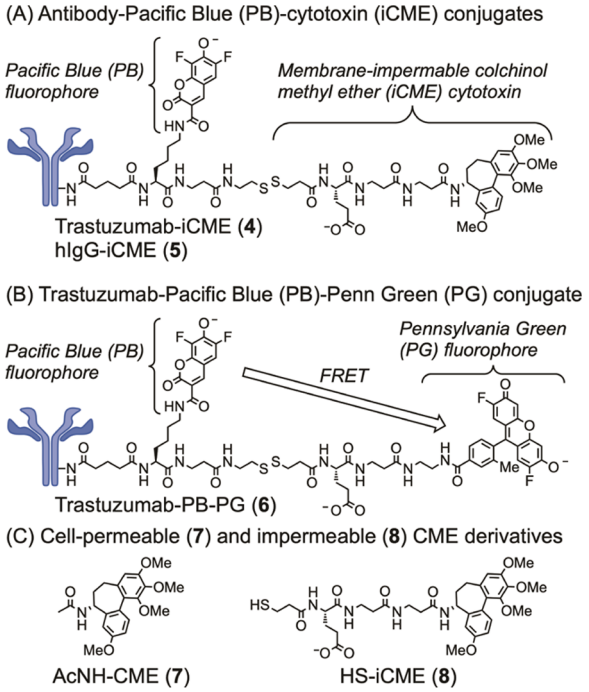

Figure 3. Structures of antibody−cytotoxin conjugates (**4**, **5**, panel A), a blue/green fluorescent trastuzumab conjugate (**6** panel B), and control compounds (**7**, **8**, panel C).

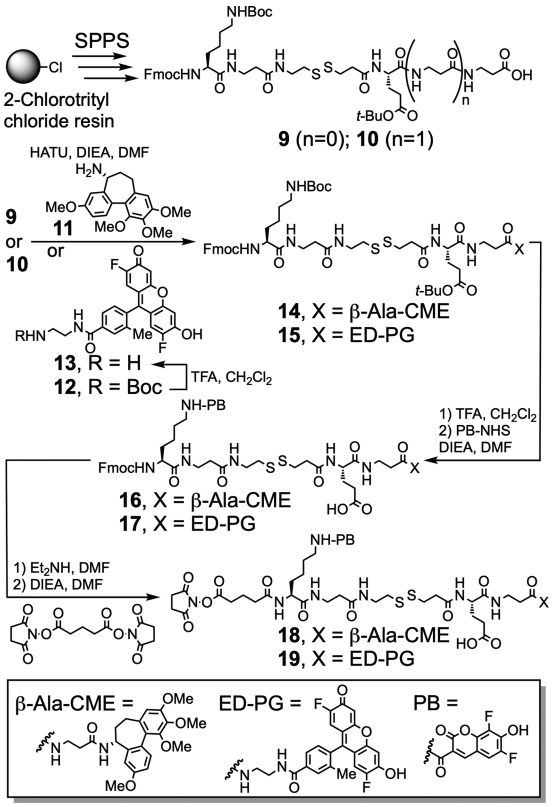

Figure 4. Synthesis of NHS esters used to prepare lysine-linked antibody conjugates **4**−**6**.

NHS esters, purified by size-exclusion chromatography, and the DOL was quantified by absorbance spectroscopy, as described in the Experimental Section. Chol-EDP (**3**) was prepared by solid-phase peptide synthesis, as described in the Experimental Section.

Biological Evaluation. We previously demonstrated that cholesterylamine-PC4 can disrupt endosomes of Jurkat lymphocyte cells (EC_{50} (14 h) = 1.3 ± 0.3 μM) and release HS-fluorescein from these compartments when cells are treated with cholesterylamine-SS-fluorescein (structures and data shown in Figure S1, Supporting Information).[32] The comparison of cholesterylamine-PC4 with the novel analogue Chol-EDP (**3**) by flow cytometry revealed that **3** is ∼30-fold more potent (EC_{50} (14 h) = 0.04 ± 0.01 μM) as a disruptor of endosomes but maintains comparably low cytotoxicity (IC_{50} (**3**, 48 h) = 11 ± 2 μM) toward Jurkat cells (Figure S1). Because of its enhanced potency, we used Chol-EDP (**3**) to investigate effects on the HER2-targeted and nontargeted fluorescent antibody conjugates **1** and **2**. As shown in Figure 5, treatment of HER2-expressing SKBR3 cells with these conjugates, and imaging by confocal laser-scanning microscopy, revealed that trastuzumab-Fl (**1**) binds with high affinity

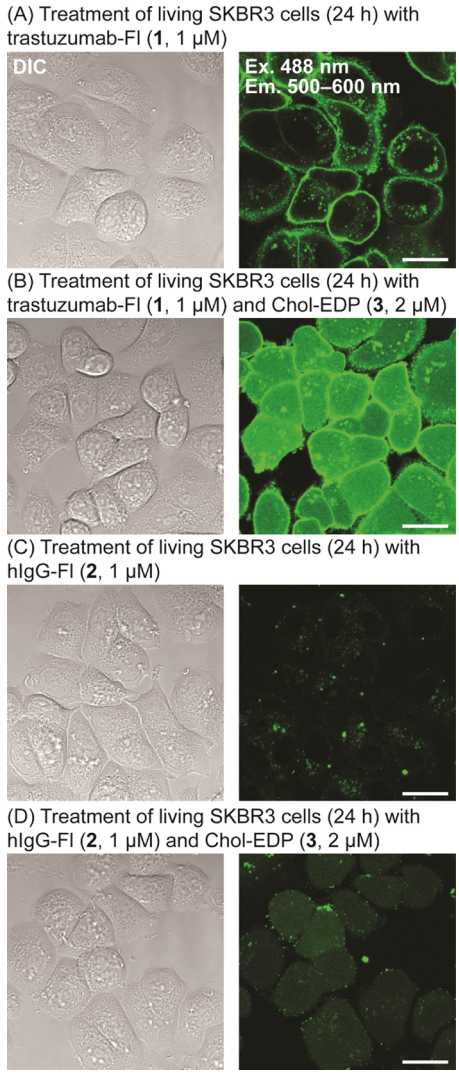

Figure 5. DIC and confocal fluorescence micrographs of living HER2+ SKBR3 cells treated with HER2-targeted (**1**) and nontargeted (**2**) fluorescent antibody conjugates (1 μM) without (A, C) and with (B, D) Chol-EDP (**3**, 2 μM) for 24 h. DOL(**1**) = 4.6. DOL(**2**) = 4.5. Scale bar = 25 μm.

DOI: 10.1021/acsomega.9b01585
ACS Omega 2019, 4, 12955−12968

and specificity to cellular plasma membranes and accumulates in intracellular compartments. Previous studies of related fluorescent trastuzumab conjugates in SKBR3 cells have revealed a very similar pattern of cellular and subcellular localization, where the intracellular compartments co-localize with the early endosomal marker transferrin.[33] Co-administration of **1** with Chol-EDP (**3**) for 24 h resulted in fluorescence dispersed throughout cells, a phenotype associated with the cleavage of the disulfide of **1**, and escape of HS-fluorescein from endosomes into the cytosol and nucleus. In contrast, the nontargeted hIgG-Fl (**2**) conferred much lower levels of cellular fluorescence in the absence and presence of **3** (Figure 5, compare A and C). However, the small amount of compartmentalized intracellular fluorescence observed with hIgG-Fl (**2**), presumably the result of some uptake by pinocytosis, was similarly dispersed throughout the cytoplasm and nucleus upon treatment with **3** (Figure 5, compare C and D). Similar studies of trastuzumab-Fl (**1**) in the HER2-negative breast cancer cell line MDA-MB-468 revealed low cellular fluorescence, consistent with the low expression of HER2 in this cell line, comparable to that observed with hIgG-Fl (**2**) in SKBR3 cells (Figure S2).

To determine whether antibody−iCME conjugates (**4**, **5**) might synergize with Chol-EDP (**3**), we evaluated effects on cellular viability. We reasoned that when the targeted conjugate **4** binds HER2 on the cell surface and undergoes endocytosis, the impermeability of the released HS-iCME (**8**) product would cause its entrapment in endosomes and lysosomes, rendering it essentially nontoxic. However, co-administration with Chol-EDP (**3**) could release **8** into the cytosol, where it could bind tubulin and block cell division. The Pacific Blue fluorophore on the protein side of the disulfide linker was used to quantify the average number of small molecules per antibody (degree of labeling, DOL), confirm the extent of binding to cells by confocal microscopy, and evaluate cellular uptake by flow cytometry (Figure S3).

To quantify cellular cytotoxicity, dose−response curves for combinations of **3**, **4**, and **5** were generated with HER2-positive SKBR3 cells and HER2-negative MDA-MB-468 cells after treatment for 72 h (Figure 6). As a positive cytotoxic control, cells were treated with *N*-acetylcolchinol methyl ether (**7**). As a cell-impermeable negative control, the anionic CME derivative **8**, predicted to result from cleavage of the disulfide of **4** and **5** (Figure 4) was evaluated. Under these conditions, cell-permeable **7** was highly toxic toward both cell lines (IC_{50} (SKBR3) = 7 ± 5 nM; IC_{50} (MDA-MB-468) = 14 ± 8 nM). In contrast, the anionic CME derivative **8** was essentially nontoxic (IC_{50} > 10 μM), consistent with low cellular permeability. As expected, the nontargeted hIgG conjugate **5** exhibited relatively low toxicity alone (IC_{50} (SKBR3) > 1 μM) toward either cell line. When this nontargeted conjugate (**5**) was combined with the essentially nontoxic Chol-EDP (**3**, IC_{50} (SKBR3) > 10 μM), held at a fixed nontoxic concentration of 2 μM, this combination was also of relatively low toxicity (IC_{50} (SKBR3) ∼ 700 nM), despite the likelihood of some uptake of this conjugate by pinocytosis. Under these same conditions, the cytotoxicity of **8** was not substantially enhanced by co-administration with 2 μM of Chol-EDP (IC_{50} (SKBR3) ∼ 7 μM; IC_{50} (MDA-MB-468) > 10 μM, data not shown). Similarly, the HER2-targeted trastuzumab conjugate **4** exhibited relatively low toxicity alone (IC_{50} (SKBR3) > 1 μM) toward HER2-positive SKBR3 cells and lower toxicity toward HER2-negative MDA-MB-468 cells (IC_{50} (MDA-MB-468) > 10 μM). In contrast, when SKBR3 cells were treated with a combination of the HER2-targeted conjugate **4** and Chol-EDP (**3**, 2 μM), this combination synergistically killed more than 90% of cells in culture with subnanomolar potency (IC_{50} (SKBR3) = 0.11 ± 0.07 nM), while maintaining relatively low toxicity toward MDA-MB-468 cells under identical conditions (IC_{50} (MDA-MB-468) > 1 μM). Consequently, Chol-EDP (**3**) enhanced the toxicity of the targeted trastuzumab-iCME (**4**) toward HER2+ SKBR3 cells by ∼10 000-fold, but it did not comparably enhance the toxicity of **4** toward HER2− MDA-MB-468 cells under the same conditions. An additional analysis of the cellular fluorescence emitted by Pacific Blue of trastuzumab-iCME (**4**) in the absence of Chol-EDP (**3**) revealed subnanomolar potency of antibody uptake by SKBR3 cells (EC_{50} = 0.5 ± 0.2 nM, Figure S3), further confirming potent binding to the HER2 antigen by this conjugate, despite its low cytotoxicity alone. In conjunction with the microscopy studies of **1**−**3** (Figure 5), these results support a mechanism of targeted synergistic cytotoxicity involving binding of the trastuzumab−iCME conjugate **4** to HER2 on SKBR3 cells, endocytosis, and release of HS-iCME (**8**) from endosomes mediated by Chol-EDP (**3**).

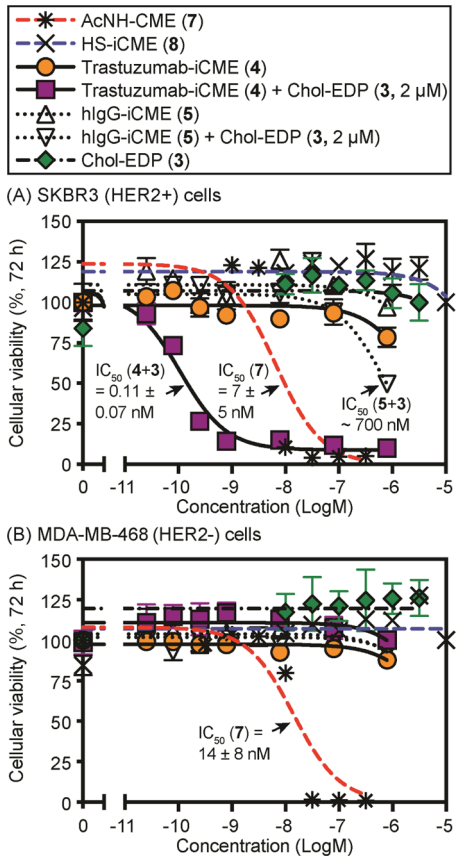

Figure 6. Quantification of cytotoxic IC_{50} values (±SEM) toward SKBR3 cells (A) and MDA-MB-468 cells (B). Cells were treated with **3**−**5** and controls **7**−**8** for 72 h and cytotoxicity was analyzed by flow cytometry. DOL(**4**) = 5.9. DOL(**5**) = 5.7.

The mechanism of disruption of endosomes by Chol-EDP (**3**) is not fully understood. However, based on previous studies of structurally related fluorescent cholesteryl carbamates[48] and cholesterylamine-PC4,[32] the insertion of the cholesterol moiety of this compound into cellular plasma

DOI: 10.1021/acsomega.9b01585
ACS Omega 2019, 4, 12955−12968

membranes is likely to allow it to engage an endocytic trafficking pathway that leads to its predominant accumulation in early and recycling endosomes. We hypothesize that the hydrophobic peptide moiety of Chol-EDP (**3**) may additionally insert into endosomal membranes to form pores that allow the escape of small molecules from these compartments, but further studies will be necessary to more precisely define its mechanism of action. To gain greater insight into the effect of Chol-EDP (**3**) on disulfide-linked antibody conjugates, we investigated effects on the trastuzumab−PB−PG conjugate **6**. This conjugate is structurally very similar to **4** but it substitutes CME with Pennsylvania Green (PG),[44,45] a highly fluorescent small molecule of comparable molecular size and hydrophobicity. Importantly, like other coumarin-fluorescein pairs,[49,50] fluorescence spectroscopy revealed that the proximal PB fluorophore of **6** undergoes Förster resonance energy transfer (FRET) with PG, providing a new FRET pair that allows cleavage of the disulfide bond between these fluorophores to be followed. When **6** was treated with the reducing agent dithiothreitol (DTT) in aqueous buffer, decreased FRET between these fluorophores and reduced fluorescence quenching resulted in enhanced blue and green fluorescence (data shown in Figure S4). A similar increase in blue fluorescence was also observed as the disulfide of **4** was cleaved, from decreased fluorescence quenching of PB by iCME (Figure S4). These effects on fluorescence allowed quantification of the half-lives associated with the cleavage of the disulfide under pseudo-first-order conditions ($t_{1/2}$ (**6**) = 307 ± 24 s; $t_{1/2}$ (**4**) = 274 ± 26 s). These studies demonstrated that the kinetics of cleavage of the disulfides of **6** and **4** are similar in aqueous buffer, but **6** additionally allows observation of the release of the green fluorescent probe as a mimic of iCME.

Confocal microscopy and flow cytometry were used to analyze the time-dependent fluorescence of SKBR3 cells treated with the targeted FRET conjugate **6** in the absence and presence of **3** (Figure 7). Immediately after addition of **6**, this conjugate can be observed bound to the plasma membrane. Over time, fluorescence accumulates intracellularly as this conjugate is endocytosed, where it presumably additionally returns to the cell surface via plasma membrane recycling. Confocal micrographs showed that green fluorescence is only released from endosomes upon treatment with both **6** and **3**; cells treated with only **6** showed exclusively compartmentalized green fluorescence, consistent with intact endosomal membranes (Figure 7). However, unlike the smaller HS-fluorescein moiety of **1**, the green fluorescent HS-Glu-PG moiety of **6** is not as extensively trapped in the cytoplasm and nucleus upon disruption of endosomes. We hypothesize that differential interactions with efflux transporters might explain this difference in cellular retention. These studies further revealed that **3** has some effects on the subcellular trafficking of **6**. In the absence of **3**, **6** is located mostly at the cell surface with minimal accumulation in endosomes. This is consistent with previously reported extensive endosomal recycling of HER2 back to the plasma membrane.[51,52] Co-treatment of **6** with **3** leads to greater accumulation of **6** within acidic intracellular compartments, presumably endosomes and lysosomes, that co-localize with LysoTracker Red DND-99 (Figure S5). The mechanism underlying this increased trafficking of the antibody conjugate to intracellular compartments is unknown, but it may enhance the release of cargo from these acidic compartments.

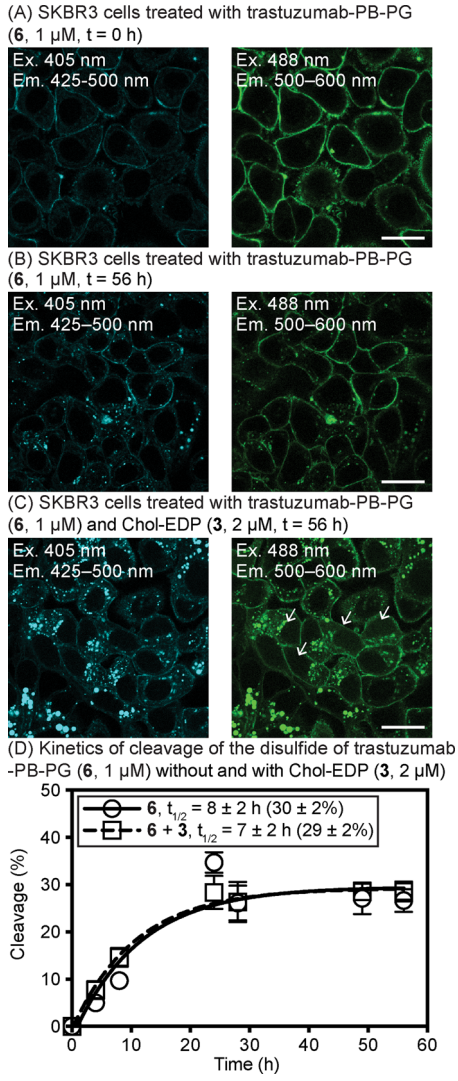

Figure 7. (A−C) Confocal micrographs of living SKBR3 cells treated with trastuzumab−PB−PG (**6**, 1 μM, DOL = 2.6). In panel A, cells were treated at 4 °C for 0.5 h prior to washing and imaging. Panels B and C: Cells were treated at 4 °C for 0.5 h prior to washing and incubation at 37 °C for 56 h in the absence (B) and presence (C) of Chol-EDP (**3**, 2 μM). In panel C, white arrows illustrate cells with dispersed green fluorescence resulting from endosome disruption and increased localization of blue and green fluorescence in endosomes/lysosomes. Scale bar = 25 μm. (D) Analysis of the kinetics of cleavage of the disulfide of **6** (DOL = 2.6) by flow cytometry. The half-time of cleavage of the disulfide of **6** and the extent of cleavage (±SEM) are not significantly altered by co-administration with **3**.

To quantify the rate of cleavage of the disulfide of **6** in endosomes, and the impact of treatment with **3**, we synthesized trastuzumab−PB−SH as a positive control for complete cleavage of the disulfide. To prepare this control, conjugate **6** was treated with excess DTT. The trastuzumab−PB−SH product was purified by size-exclusion chromatography to remove HS-PG and DTT, and the loss of green fluorescence and increased blue fluorescence was confirmed by fluorescence spectroscopy (data not shown). The analysis of a related trastuzumab−PB conjugate by flow cytometry under the same conditions demonstrated that this treatment did not adversely affect potency for HER2 on SKBR3 cells, but binding efficacy was reduced by ∼17% (Figure S4), and this difference was factored into the analysis of the kinetics of disulfide

DOI: 10.1021/acsomega.9b01585
ACS Omega 2019, 4, 12955−12968

cleavage in cells. Cells treated with trastuzumab−PB−SH were compared with cells treated with **6** in the absence and presence of **3** to measure the half-time of the cleavage reaction. These studies revealed that Chol-EDP (**3**) does not significantly affect the cleavage of **6** in endosomes ($t_{1/2}$ (**6**) = 8 ± 2 h; $t_{1/2}$ (**6** + **3**) = 7 ± 2 h). The similarity of these values suggests that despite facilitating the efflux of small molecules from endosomes, **3** does not promote substantial influx of cytosolic GSH into endosomes to promote disulfide cleavage. A similar 6 h half-life of a folate receptor-targeted FRET probe in KB cells was previously reported by Low and co-workers.[53] We found that the disulfide of **6** is maximally cleaved by ∼30% in endosomes, and this cleavage did not increase appreciably from 24 to 72 h. When endosomes were pre-permeabilized by treatment with **3** for 24 h prior to addition of **6**, similar results were obtained (data not shown), further indicating a lack of association between the cleavage of the disulfide bond and endosome disruption. This partial cleavage is consistent with another report[54] describing less than 50% cleavage when HER2-positive breast cancer cells are treated with trastuzumab emtansine disulfide for 20 h. Additionally, when maytansine DM1 is conjugated to IgG via disulfide-containing linkers, this drug is cleaved from the antibody with half-lives of 15−218 h, depending on the extent of a steric hindrance about the disulfide bond.[17,55] Other studies of trastuzumab conjugates have indicated that recycling endosomes, late endosomes, and lysosomes are oxidizing in SKBR3 cells, and cleavage of disulfides can be inefficient.[56] Consequently, subtle structural elements are likely to play a major role in the cleavage of disulfide linkers within the endosomal pathway. Other HER2-targeted antibody conjugates cleaved by cathepsin proteases have been shown by FRET to be cleaved by 41% after 20 h in SKBR3 cells.[51]

CONCLUSIONS

We report a remarkable cytotoxic synergy between a cell-impermeable antibody−drug conjugate and an endosome-disruptive peptide. The trastuzumab−iCME conjugate **4** (cytotoxic IC_{50} (SKBR3, 72 h) > 1 μM) and endosome-disruptive peptide Chol-EDP (**3**, cytotoxic IC_{50} (SKBR3, 72 h) > 10 μM) exhibit relatively low toxicity individually, but when combined potently kill more than 90% of targeted cancer cells that express HER2 (cytotoxic IC_{50} (SKBR3, 72 h) = 0.11 ± 0.07 nM). Mechanistic studies of a structurally related green fluorescent antibody conjugate support a mechanism of synergy involving binding of these trastuzumab conjugates to HER2 on cell surfaces, receptor-mediated endocytosis, and cleavage of the disulfide bond in the lumen of endosomes, with a half-life of 8 ± 2 h. When the trastuzumab−iCME conjugate **4** is added alone, cleavage of the disulfide in endosomes yields a membrane-impermeable thiol (HS-iCME, **8**) that remains trapped in the lumen, limiting cytotoxicity. However, when cells are treated with Chol-EDP (**3**), this lipopeptide initially associates with the cellular plasma membrane but subsequently traffics to endosomes, where it appears to slowly permeabilize endosomal membranes (studies of the release of fluorescence from conjugate **1** mediated by **3** indicate that substantial endosomal escape requires >8 h). This permeabilization of endosomal membranes by Chol-EDP (**3**) enables the release of the highly polar HS-iCME (**8**), delivered by trastuzumab-iCME (**4**), from endosomes into the cytoplasm and nucleus, allowing **8** to disrupt microtubules and block cell division.

The low toxicity of Chol-EDP (**3**) suggests that this peptide may create small pores in endosomal membranes that do not adversely affect cellular viability. However, if this mechanism is operational, these pores must be sufficiently large to allow the escape of HS-fluorescein and HS-iCME (**8**) from endosomes into the cytoplasm. Surprisingly, studies of the structurally similar FRET probe **6** revealed that Chol-EDP (**3**) does not affect the cleavage of the disulfide of **4**, suggesting that this compound does not appear to trigger massive influx of reduced glutathione (GSH), present in high concentrations (0.5−10 mM)[57] in the cytosol, into endosomes. Because endosomes and lysosomes have been reported to be oxidizing,[56] thiol reductases[58] in these compartments presumably mediate cleavage of disulfides. Products of proteolytic cleavage and disulfide reduction have been previously detected in cells treated with antibody−disulfide conjugates,[54] and proteolysis could potentially also contribute to this release of cargo. We found that Chol-EDP (**3**) additionally affects the trafficking and subcellular localization of trastuzumab conjugates by increasing their accumulation in acidic intracellular compartments, and this altered trafficking may play a role in enhancing endosomal escape.

Given the recent interest[22,23] in triggering the release of small molecules from antibodies and previous studies of delivery of toxins using endosome-disruptive agents,[31] the approach described here has the potential to improve the properties of ADCs. Cell-impermeable toxins that can be activated by other nontoxic compounds may reduce side effects associated with premature release and diffusion of toxins into nontargeted cells. Alternatively, pretargeting, involving treatment and wash-out of the ADC followed by subsequent administration of an endosome-disruptive peptide, might improve the therapeutic index of some of these types of agents.

EXPERIMENTAL SECTION

General Experimental Section. Chemical reagents were purchased from Aapptec, Acros, Aldrich, Alfa Aesar, EMD Biosciences, or TCI America and were used without further purification. Solvents were from Aldrich or Fisher Scientific. 3-((((Cholester-3-yl)oxy)carbonyl)amino)propanoic acid,[59] 3-((2-(((9*H*-fluoren-9-ylmethoxy)carbonyl)amino)ethyl)-dithio)propanoic acid,[32,60] and Pacific Blue NHS ester (PB-NHS)[61] were prepared as previously described. Analytical reverse-phase (RP) HPLC employed an Agilent 1220 Series binary pump and an Agilent PLRP-S RP analytical column (8 μm particle size, 4 mm × 25 cm) with diode-array detection at 254 nm. Preparative RP-HPLC employed an Agilent 1200 or 1260 Series preparative pump/gradient extension with a Hamilton PRP-1 (polystyrene-divinylbenzene) RP preparative column (10−12 μm particle size, 21.5 mm × 25 cm, flow rate of 25.0 or 16.0 mL/min with a gradient (0.1% TFA) of H_2O/MeCN, 9:1 (1 min) to 0:100 (24 min), 0:100 (5 min), 9:1 (5 min)). HPLC fractions containing water were dried using a Labconco FreeZone 4.5 lyophilizer. Compounds containing basic amines were isolated as TFA salts. Nuclear magnetic resonance (NMR) spectra were recorded on a 500 MHz Bruker Avance spectrometer with a dual carbon/proton cryoprobe. Chemical shifts are reported in parts per million (ppm) and are referenced to the center line of the solvent (DMSO-d_6: ^{1}H, 2.50 ppm, ^{13}C 39.51 ppm). Coupling constants are given in Hertz (Hz). Spin multiplicities are reported as s = singlet, d = doublet, t = triplet, q = quartet, dd = doublet of doublet, td = doublet of triplet, and m = multiplet.

DOI: 10.1021/acsomega.9b01585
ACS Omega 2019, 4, 12955−12968

SPPS was performed on a Mettler Toledo MiniBlock reactor (model no: Bohdan 2080 on a 12-well block with glass reaction vessels, 600 rpm) utilizing standard Fmoc chemistry.

Synthetic Procedures and Compound Characterization Data. *((3β-Cholest-5-en-3-yl)carbonyl)-β-alanyl-β-alanyl-L-glutamyl-L-glutamyl-mPEG-mPEG-aminoisobutyl-aminoisobutyl-aminoisobutyl-aminoisobutyl-L-tryptophyl-L-tyrosyl-L-alanyl-L-tryptophyl-L-tyrosyl-L-alanyl-L-tryptophyl-L-tyrosyl-L-prolyl-L-prolyl-L-valyl-L-valinamide (Chol-EDP, **3**).* SPPS was performed on Rink amide MBHA resin (0.5 mmol/g, 40 mg, 0.02 mmol) swelled in DMF for 2 h. The removal of the Fmoc group was accomplished by agitating with the deblocking solution (20% piperidine in DMF, 2 mL, 2×, for 4 min each). The resin was washed with DMF (2 mL, 4×) to remove any traces of piperidine and treated with Fmoc-amino acids (4 equiv), HATU (3.8 equiv), and DIEA (8 equiv) in DMF (2 mL) with agitation until coupling was complete by Kaiser Test (3, 6, 12, or 16 h). Once the coupling was complete, the reaction solution was drained, and the resin was washed four times with DMF (2 mL). This coupling protocol was repeated for each additional Fmoc-amino acid. The hindered 2-aminoisobutyric acid (Aib) was coupled as the acid fluoride (Fmoc-Aib-F), synthesized using DAST.[62] Fmoc-Aib-F (4 equiv) was dissolved in DMF (0.5 mL), added to the resin, and agitated for 6 h. Coupling to 3-((((cholester-3-yl)oxy)carbonyl)amino)propanoic acid,[59] cleavage with TFA/H_2O/TIPS (95/2.5/2.5) with agitation for 2 h, and purification by RP-HPLC provided **3** as a white solid (15 mg, 0.005 mmol, 24% overall yield). LRMS (ESI−) m/z calcd for $C_{164}H_{232}N_{26}O_{37}$ $[(M - 2H)/2]^-$: 1578.3, found: 1578.8.

5-((2-((3-((2,5-Dioxopyrrolidin-1-yl)oxy)-3-oxopropyl)disulfanyl)ethyl)carbamoyl)-2-(6-hydroxy-3-oxo-3H-xanthen-9-yl)benzoic Acid (This Compound is Also Termed Here 5-Carboxyfluorescein-disulfide-NHS Ester). 3-((2-(((9*H*-Fluoren-9-ylmethoxy)carbonyl)amino)ethyl)dithio)propanoic acid[32,60] (28 mg, 0.070 mmol) was dissolved in DMF (1 mL) containing 20% piperidine and stirred at 22 °C for 30 min. The solvent was removed under vacuum to provide the primary amine. 5-Carboxyfluorescein NHS ester (17 mg, 0.035 mmol) dissolved in dry DMF (2 mL) was added. DIEA (0.2 mL) was added, and the reaction was stirred at 22 °C for 16 h. The solvent was removed under vacuum, the residue was dissolved in CH_2Cl_2 containing 5% methanol, applied to a short silica plug, and eluted with CH_2Cl_2/MeOH (9:1). The solvent was removed under vacuum to give the crude carboxylic acid. This product (∼15 mg) was dissolved in DMF (2 mL), and EDC (11 mg, 0.06 mmol), *N*-hydroxysuccinimide (7 mg, 0.06 mmol) were added. The reaction was stirred at 22 °C for 16 h. The solvent was removed under vacuum, the residue was dissolved in DMSO (2 mL), and the product was purified by preparative RP-HPLC. Pure fractions were collected, combined, and dried under vacuum to give 5-carboxyfluorescein-disulfide-NHS ester (9 mg, 0.014 mmol, 39% overall yield) as a yellow solid. ^{1}H NMR (500 MHz, DMSO-d_6) δ 9.01 (t, J = 5.5 Hz, 1H), 8.46 (s, 1H), 8.25 (d, J = 7.9, 1.6 Hz, 1H), 7.38 (d, J = 8.0 Hz, 1H), 6.69 (d, J = 1.9 Hz, 2H), 6.59 (d, J = 8.6 Hz, 2H), 6.56−6.53 (m, 2H), 3.62 (q, J = 6.3 Hz, 2H), 3.13 (t, J = 6.5 Hz, 2H), 3.05 (t, J = 6.9 Hz, 2H), 2.98 (t, J = 6.6 Hz, 2H), 2.54 (s, 4H). ^{13}C NMR (126 MHz, DMSO-d_6) δ 170.1, 168.2, 167.5, 164.8, 159.6, 154.7, 151.8, 136.0, 134.7, 129.2, 126.5, 124.3, 123.3, 112.7, 109.1, 102.3, 40.4, 36.9, 31.9, 30.4, 25.4. HRMS (ESI+) m/z calcd for $C_{30}H_{24}N_2O_{10}S_2$ $[M + Na]^+$: 659.0765, found: 659.0740.

*(4S)-4-(3-Mercaptopropanamido)-5-oxo-5-((3-oxo-3-((3-oxo-3-(((5R)-3,9,10,11-tetramethoxy-6,7-dihydro-5H-dibenzo[a,c][7]annulen-5-yl)amino)propyl)amino)propyl)-amino)pentanoic Acid (HS-iCME, **8**).* Disulfide **18** (6 mg, 0.004 mmol) was dissolved in DMSO (0.4 mL). DL-Dithiothreitol (DTT, 13 mg, 0.085 mmol) was added, and the solution was stirred at room temperature (22 °C) for 16 h. The crude mixture was purified by RP-HPLC and lyophilized to yield HS-iCME (**8**) as a white solid (2 mg, 68% yield). ^{1}H NMR (500 MHz, DMSO-d_6) δ 8.39 (d, J = 8.4 Hz, 1H), 8.10 (d, J = 8.0 Hz, 1H), 8.05 (d, J = 8.1 Hz, 1H), 7.89 (dt, J = 10.9, 5.8 Hz, 2H), 7.24 (d, J = 8.1 Hz, 1H), 6.87 (d, J = 8.2 Hz, 1H), 6.77 (s, 1H), 4.57−4.48 (m, 1H), 4.0 (td, J = 8.4, 5.4 Hz, 1H), 3.82 (s, 3H), 3.78 (s, 3H), 3.77 (s, 3H), 3.47, (s, 3H), 3.30−3.12 (m, 4H), 2.95−2.85 (m, 1H), 2.78−2.68 (m, 1H), 2.68−2.60 (m, 1H), 2.49−2.41 (m, 2H), 2.37−2.28 (m, 2H), 2.24−2.13 (m, 4H), 2.10−1.99 (m, 1H), 1.88 (d, J = 6.1 Hz, 2H), 1.77−1.63 (m, 2H), 1.30−1.21 (m, 1H). ^{13}C NMR (126 MHz, DMSO) δ 173.9, 171.2, 170.4, 170.3, 169.6, 158.4, 152.1, 150.3, 141.8, 140.6, 134.8, 130.5, 126.1, 124.3, 110.8, 109.3 108.0, 60.5, 55.8, 54.9, 51.9, 48.2, 40.0, 39.9, 39.7, 39.5, 39.3, 39.2, 39.0, 38.3, 35.4, 35.3, 35.3, 35.1, 30.2, 30.2, 27.4, 25.2, 19.9. HRMS (ESI+) m/z calcd for $C_{33}H_{44}N_4O_{10}S$ $[M + H]^+$: 689.2856, found: 689.2849.

*(10S,25S)-10-((((9H-Fluoren-9-yl)methoxy)carbonyl)-amino)-25-(3-(tert-butoxy)-3-oxopropyl)-2,2-dimethyl-4,11,15,23,26-pentaoxo-3-oxa-19,20-dithia-5,12,16,24,27-pentaazatriacontan-30-oic Acid (**9**).* 2-Chlorotrityl chloride resin (2-CTC, Aapptec, RTZ001, 0.1 mmol) was allowed to swell in CH_2Cl_2 (10 min). The first Fmoc-L-amino acid (4 eq) in dry CH_2Cl_2 (4 mL) containing DIEA (8 eq) was added to the MiniBlock reactor with agitation for 16 h. The resin was washed with CH_2Cl_2 (4 mL, 4×) followed by MeOH (4 mL) with agitation (10 min) to cap any unreacted resin. The solvent was removed, and the resin was washed with DMF (4 mL, 4×). Additional coupling steps were performed as described for the preparation of **3** on Rink amide resin, with the exception of the disulfide amino acid, which was added as the acid fluoride. Briefly, Fmoc-protected 3-((2-aminoethyl)-disulfanyl)propanoic acid (80 mg, 0.2 mmol) was dissolved in dry CH_2Cl_2 (2 mL) in a polypropylene conical tube (15 mL). Drops of dry DMF were added until the solution cleared, followed by the addition of DAST (63 μL, 0.48 mmol). The reaction was stirred for 30 min at 4 °C and was quenched by the addition of ice water. The organic layer was washed with satd. aqueous NaCl and dried over anhydrous Na_2SO_4. The crude material was concentrated under reduced pressure and redissolved in DMF. The resulting solution was immediately added to the resin with agitation for 16 h. Cleavage of **9** from 2-CTC resin was accomplished by treatment with CH_2Cl_2/TFE/acetic acid (7:2:1, 4 mL) with shaking for 3 h. The resin was removed by filtration and washed with CH_2Cl_2 (2 mL, 3×) and DMF (2 mL, 3×). The filtrates were combined and concentrated under vacuum to give crude products. Purification by RP-HPLC yielded **9** as a white solid (34 mg, 35% yield). ^{1}H NMR (500 MHz, DMSO-d_6) 12.23 (brs, 1H), 8.09 (d, J = 8.1 Hz, 1H), 8.05 (t, J = 5.7 Hz, 1H), 7.94 (t, J = 5.6 Hz, 1H), 7.89 (d, J = 7.4 Hz, 3H), 7.72 (t, J = 6.5 Hz, 2H), 7.42 (t, J = 7.4 Hz, 3H), 7.33 (t, J = 7.5 Hz, 2H), 6.75 (t, J = 5.9 Hz, 1H), 4.31−4.18 (m, 5H), 3.93−3.84 (m, 2H), 3.35−3.17 (m, 6H), 2.93−2.83 (m, 4H), 2.75 (t, J = 6.9 Hz, 2H), 2.54 (q, J = 4.0, 3.1 Hz, 2H), 2.37 (t, J = 6.9 Hz, 2H), 2.24 (t, J = 7.0 Hz, 2H), 2.22−2.15 (m, 2H), 1.88−1.80 (m, 1H), 1.72−

DOI: 10.1021/acsomega.9b01585
ACS Omega 2019, 4, 12955−12968

1.63 (m, 1H), 1.61−1.52 (m, 2H), 1.37 (s, 9H), 1.36 (s, 9H), 1.27−1.16 (m, 1H). ^{13}C NMR (126 MHz, DMSO) δ 172.8, 171.9, 171.6, 171.0, 170.4, 170.1, 155.9, 155.6, 143.9, 143.8, 140.7, 127.6, 127.1, 125.3, 120.1, 79.7, 77.3, 65.6, 54.7, 51.7, 46.7, 40.0, 39.8, 39.7, 39.5, 39.3, 39.2, 39.0, 37.9, 37.1, 35.2, 35.2, 34.9, 34.8, 33.9, 33.7, 31.7, 31.3, 29.2, 283, 27.7, 27.45 22.9. MS (ESI+) m/z calcd for $C_{46}H_{66}N_6O_{12}S_2$ $[M + H]^+$: 959.4258, found: 959.4267.

*(10S,25S)-10-((((9H-Fluoren-9-yl)methoxy)carbonyl)amino)-25-(3-(tert-butoxy)-3-oxopropyl)-2,2-dimethyl-4,11,15,23,26,30-hexaoxo-3-oxa-19,20-dithia-5,12,16,24,27,31-hexaazatetratriacontan-34-oic Acid (**10**).* Using 2-chlorotrityl resin (0.1 mmol) and the coupling conditions and building blocks described for **9**, the crude mixture was purified by RP-HPLC and lyophilized to provide **10** as a white solid (50 mg, 49% yield). ^{1}H NMR (500 MHz, DMSO-d_6) 12.20 (brs, 1H), 8.15−8.00 (m, 2H), 7.96−7.84 (m, 5H), 7.73 (t, J = 6.5 Hz, 2H), 7.42 (t, J = 7.3 Hz, 3H), 7.33 (t, J = 7.7 Hz, 2H), 6.76 (t, J = 5.9 Hz, 1H), 4.34−4.13 (m, 5H), 3.97−3.81 (m, 2H), 3.47−3.11 (m, 8H), 3.00−2.81 (m, 4H), 2.75 (t, J = 6.9 Hz, 2H), 2.56−2.51 (m, 2H), 2.36 (t, J = 7.1 Hz, 2H), 2.30−2.11 (m, 6H), 1.93−1.76 (m, 1H), 1.76−1.62 (m, 1H), 1.62−1.43 (m, 2H), 1.37 (s, 9H), 1.36 (s, 9H), 1.29−1.15 (m, 2H). ^{13}C NMR (126 MHz, DMSO-d_6) δ 172.9, 171.9, 171.6, 170.9, 170.4, 170.3, 170.1, 155.9, 155.5, 143.9, 143.8, 140.7, 127.6, 127.0, 125.3, 120.1, 79.6, 77.3, 65.6, 54.7, 51.8, 46.7, 37.9, 37.1, 35.3, 35.2, 35.2, 35.0, 34.9, 34.7, 33.9, 33.8, 31.7, 31.3, 29.2, 28.3, 27.7, 27.5, 22.8. LRMS (ESI+) m/z calcd for $C_{49}H_{71}N_7O_{13}S_2$ $[M + H]^+$: 1030.5, found: 1030.5.

*tert-Butyl (2-(4-(2,7-Difluoro-6-hydroxy-3-oxo-3H-xanthen-9-yl)-3-methylbenzamido)ethyl)carbamate (**12**).* To a solution of 4-carboxy Pennsylvania Green succinimidyl ester (95 mg, 0.2 mmol), prepared as previously reported,[45,63] in DMF (1 mL) were added DIEA (125 μL, 0.5 mmol) and *N*-Boc-ethylenediamine (47 μL, 0.3 mmol). The reaction mixture was stirred at 22 °C for 4 h. Solvents were removed under reduced pressure followed by purification by silica gel chromatography (eluent: CH_2Cl_2/MeOH (15:1) with 1% acetic acid) to afford **12** (78 mg, 75%) as an orange solid. ^{1}H NMR (500 MHz, DMSO-d_6) δ 8.60 (t, J = 5.7 Hz, 1H), 7.96 (s, 1H), 7.88 (d, J = 7.9 Hz, 1H), 7.38 (d, J = 7.9 Hz, 1H), 6.92 (t, J = 5.8 Hz, 1H), 6.84 (d, J = 6.6 Hz, 2H), 6.61 (d, J = 11.1 Hz, 2H), 3.34 (q, J = 6.2 Hz, 2H), 3.15 (q, J = 6.3 Hz, 2H), 2.08 (s, 3H), 1.38 (s, 9H). ^{13}C NMR (126 MHz, DMSO-d_6) δ 165.83, 155.78, 149.38, 149.33, 149.28, 135.93, 135.75, 134.27, 129.53, 129.02, 125.13, 111.35, 105.15, 105.12, 77.69, 40.42, 28.22, 19.08. HRMS (ESI−) m/z calcd for $C_{28}H_{25}F_2N_2O_6$ $[M-H]^-$: 523.1681, found: 523.1668.

*tert-Butyl-(10S,25S)-10-((((9H-fluoren-9-yl)methoxy)carbonyl)amino)-2,2-dimethyl-4,11,15,23-tetraoxo-25-((3-oxo-3-((3-oxo-3-(((5R)-3,9,10,11-tetramethoxy-6,7-dihydro-5H-dibenzo[a,c][7]annulen-5-yl)amino)propyl)amino)propyl)carbamoyl)-3-oxa-19,20-dithia-5,12,16,24-tetraazaoctacosan-28-oate (**14**).* To a solution of **10** (40 mg, 0.039 mmol) in dry DMF (2 mL) were added HATU (30 mg, 0.078 mmol), DIEA (35 μL, 0.19 mmol), and CME (**11**, 26 mg, 0.078 mmol). The mixture was stirred overnight and concentrated under reduced pressure. The crude material was purified by RP-HPLC and lyophilized to afford **14** as a white solid (38 mg, 73% yield). ^{1}H NMR (500 MHz, DMSO-d_6) 8.39 (d, J = 8.4 Hz, 1H), 8.13−8.00 (m, 2H), 7.94−7.84 (m, 5H), 7.72 (t, J = 6.6 Hz, 2H), 7.45−7.36 (m, 3H), 7.32 (t, J = 7.5 Hz, 2H), 7.24 (d, J = 8.1 Hz, 1H), 6.90−6.83 (m, 2H), 6.81−6.69 (m, 2H), 4.52 (dt, J = 11.9, 7.6 Hz, 1H), 4.35−4.15 (m, 5H), 3.95−3.84 (m, 2H), 3.82 (s, 3H), 3.77 (s, 3H), 3.77 (s, 3H), 3.47 (s, 3H), 3.34−3.15 (m, 8H), 2.88 (tt, J = 6.9, 4.4 Hz, 4H), 2.75 (t, J = 7.0 Hz, 2H), 2.59−2.52 (m, 2H), 2.48−2.45 (m, 1H), 2.39−2.27 (m, 2H), 2.27−2.09 (m, 7H), 2.09−1.98 (m, 1H), 1.91−1.76 (m, 2H), 1.72−1.62 (m, 1H), 1.61−1.43 (m, 2H), 1.36 (s, 9H), 1.36 (s, 9H), 1.29−1.14 (m, 2H). ^{13}C NMR (126 MHz, DMSO-d_6) δ 171.9, 171.3, 170.9, 170.4, 170.2, 170.1, 169.6, 158.4, 155.9, 152.1, 150.3, 143.9, 143.8, 141.8, 140.7, 140.6, 134.7, 130.5, 127.6, 127.1, 126.1, 125.3, 124.3, 120.1, 110.8, 109.3, 108.1, 79.7, 77.3, 65.6, 60.5, 55.8, 54.9, 54.7, 51.8, 48.2, 46.7, 38.3, 37.9, 37.1, 35.4, 35.3, 35.3, 35.2, 35.2, 35.1, 34.9, 33.9, 31.7, 31.3, 30.1, 29.2, 28.3, 27.7, 27.5, 22.9. LRMS (ESI+) m/z calcd for $C_{68}H_{92}N_8O_{16}S_2$ $[M + H]^+$: 1341.6, found: 1341.7.

*tert-Butyl (10S,25S)-10-((((9H-Fluoren-9-yl)methoxy)carbonyl)amino)-25-((3-((2-(4-(2,7-difluoro-6-hydroxy-3-oxo-3H-xanthen-9-yl)-3-methylbenzamido)ethyl)amino)-3-oxopropyl)carbamoyl)-2,2-dimethyl-4,11,15,23-tetraoxo-3-oxa-19,20-dithia-5,12,16,24-tetraazaoctacosan-28-oate (**15**).* To a solution of **9** (34 mg, 0.035 mmol) in dry DMF (1 mL) were added HATU (27 mg, 0.071 mmol) and DIEA (33 μL, 0.18 mmol). Separately, **12** (37 mg, 0.071 mmol) was treated with TFA/CH_2Cl_2 (0.5 mL, 1:1) for 30 min. The mixture was concentrated under reduced pressure and washed with CH_2Cl_2 (2 mL, 4×) to remove excess TFA and afford **13** as the crude amine. This crude amine was dissolved in dry DMF (0.5 mL) and added to the solution of HATU-activated carboxylic acid. The mixture was stirred for 16 h, and the solvent was removed with a Biotage V-10 Touch. Purification by RP-HPLC followed by lyophilization afforded **15** as an orange solid (17 mg, 36% yield). ^{1}H NMR (500 MHz, DMSO-d_6) δ 8.67 (t, J = 5.7 Hz, 1H), 8.10 (d, J = 8.0 Hz, 1H), 8.07−8.00 (m, 3H), 7.98−7.86 (m, 7H), 7.72 (t, J = 6.5 Hz, 2H), 7.45−7.35 (m, 4H), 7.32 (t, J = 7.7 Hz, 2H), 6.85 (d, J = 7.0 Hz, 2H), 6.75 (t, J = 5.2 Hz, 1H), 6.61 (d, J = 11.1 Hz, 2H), 4.31−4.13 (m, 5H), 3.89 (p, J = 7.2 Hz, 1H), 3.40−3.17 (m, 10H), 2.93−2.82 (m, 4H), 2.74 (t, J = 6.9 Hz, 1H), 2.59−2.51 (m, 1H), 2.34−2.12 (m, 6H), 2.08 (s, 3H), 1.88−1.79 (m, 1H), 1.75−1.64 (m, 1H), 1.62−1.47 (m, 2H), 1.36 (s, 9H), 1.35 (s, 9H), 1.27−1.21 (m, 2H). ^{13}C NMR (126 MHz, DMSO-d_6) δ 171.9, 171.6, 171.1, 171.0, 170.6, 170.6, 170.4, 170.2, 165.9, 158.4, 158.1, 157.8, 155.9, 155.6, 143.9, 143.8, 140.7, 136.0, 135.7, 134.3, 129.6, 129.1, 127.6, 127.1, 125.3, 125.1, 120.1, 116.6, 114.3, 105.1, 79.6, 77.3, 65.6, 54.7, 51.8, 46.7, 40.0, 39.8, 39.7, 39.5, 39.3, 39.2, 39.0, 38.3, 37.9, 37.1, 35.4, 35.3, 35.2, 34.9, 33.9, 33.3, 31.7, 31.3, 31.3, 29.2, 28.3, 27.7, 27.5, 22.9, 19.10. LRMS (ESI+) m/z calcd for $C_{69}H_{82}F_2N_8O_{15}S_2$ $[M + H]^+$: 1365.5, found: 1365.5.

*(5S,20S)-5-(4-(6,8-Difluoro-7-hydroxy-2-oxo-2H-chromene-3-carboxamido)butyl)-1-(9H-fluoren-9-yl)-3,6,10,18-tetraoxo-20-((3-oxo-3-((3-oxo-3-(((5R)-3,9,10,11-tetramethoxy-6,7-dihydro-5H-dibenzo[a,c][7]annulen-5-yl)amino)propyl)amino)propyl)carbamoyl)-2-oxa-14,15-dithia-4,7,11,19-tetraazatricosan-23-oic Acid (**16**).* **14** (30 mg, 0.022 mmol) was dissolved in TFA/CH_2Cl_2 (1:3, 2 mL) and stirred for 2 h. The solvent was removed under reduced pressure, and the solid was dissolved in dry DMF (2 mL). Pacific Blue NHS ester (PB-NHS, 11 mg, 0.034 mmol) and DIEA (8 μL, 0.045 mmol) were added. The solution was stirred for 16 h, and the solvent was removed under reduced pressure. The crude material was purified by RP-HPLC and

DOI: 10.1021/acsomega.9b01585
ACS Omega 2019, 4, 12955−12968

lyophilized to afford **16** as a yellow solid (21 mg, 67% yield). ^{1}H NMR (500 MHz, DMSO-d_6) 12.08 (brs, 1H), 8.75 (s, 1H), 8.59 (t, J = 5.8 Hz, 1H), 8.39 (d, J = 8.4 Hz, 1H), 8.09 (d, J = 8.1 Hz, 1H), 8.04 (t, J = 5.7 Hz, 1H), 7.97−7.88 (m, 3H), 7.85 (dd, J = 7.6, 3.8 Hz, 2H), 7.70 (t, J = 7.8 Hz, 3H), 7.45 (d, J = 8.3 Hz, 1H), 7.42−7.36 (m, 2H), 7.35−7.27 (m, 2H), 7.24 (d, J = 8.2 Hz, 1H), 6.90−6.83 (m, 2H), 6.76 (s, 1H), 4.57−4.48 (m, 1H), 4.35−4.26 (m, 1H), 4.23−4.12 (m, 4H), 3.96−3.89 (m, 1H), 3.82 (s, 3H), 3.77 (s, 3H), 3.76 (s, 3H), 3.47 (s, 3H), 3.34−3.14 (m, 10H), 2.94−2.81 (m, 2H), 2.79−2.70 (m, 2H), 2.56−2.51 (m, 2H), 2.48−2.43 (m, 1H), 2.39−2.28 (m, 2H), 2.27−2.10 (m, 7H), 2.09−1.98 (m, 1H), 1.92−1.80 (m, 2H), 1.74−1.58 (m, 2H), 1.58−1.44 (m, 3H), 1.40−1.25 (m, 2H). ^{13}C NMR (126 MHz, DMSO-d_6) δ 173.9, 171.9, 171.0, 170.4, 170.3, 170.1, 169.6, 160.9, 159.6, 158.4, 158.3, 158.0, 157.77, 157.5, 155.9, 152.1, 150.3, 147.9, 147.1, 143.8, 141.8, 140.7, 140.6, 140.5, 134.7, 130.5, 127.6, 127.6, 127.0, 126.1, 125.34, 125.3, 124.3, 120.1, 117.7, 116.4, 110.8, 110.5, 110.4, 109.6, 109.4, 109.3, 108.1, 65.6, 60.5, 55.8, 54.9, 54.5, 51.9, 48.2, 46.7, 38.3, 37.9, 37.1, 35.4, 35.3, 35.3, 35.2, 35.1, 34.9, 33.9, 31.7, 30.2, 30.1, 28.7, 27.5, 23.0. LRMS (ESI+) m/z calcd for $C_{69}H_{78}F_2N_8O_{18}S_2$ $[M + H]^+$: 1409.5, found: 1409.5.

*(5S,20S)-20-((3-((2-(4-(2,7-Difluoro-6-hydroxy-3-oxo-3H-xanthen-9-yl)-3-methylbenzamido)ethyl)amino)-3-oxopropyl)carbamoyl)-5-(4-(6,8-difluoro-7-hydroxy-2-oxo-2H-chromene-3-carboxamido)butyl)-1-(9H-fluoren-9-yl)-3,6,10,18-tetraoxo-2-oxa-14,15-dithia-4,7,11,19-tetraazatricosan-23-oic Acid (**17**).* **15** (17 mg, 0.012 mmol) was dissolved in TFA/CH_2Cl_2 (1:3, 2 mL) and stirred for 2 h. The solvent was removed under reduced pressure, and the residue was washed with CH_2Cl_2 to remove all traces of acid (2 mL, 3×). The product was dissolved in dry DMF (1.5 mL), and PB-NHS (9 mg, 0.029 mmol) and DIEA (14 μL, 0.080 mmol) were added. The solution was stirred for 16 h, and the solvent was removed with a Biotage V-10 Touch. The crude product was purified by RP-HPLC to afford **17** as a yellow solid (6 mg, 34% yield). ^{1}H NMR (500 MHz, DMSO-d_6) δ 8.74 (s, 1H), 8.67 (t, J = 5.6 Hz, 1H), 8.58 (t, J = 5.8, 5.3 Hz, 1H), 8.11 (d, J = 8.0 Hz, 1H), 8.04 (q, J = 6.0 Hz, 2H), 7.98−7.90 (m, 3H), 7.89 (d, J = 8.1 Hz, 1H), 7.86−7.82 (m, 2H), 7.73−7.66 (m, 3H), 7.44 (d, J = 8.2 Hz, 1H), 7.41−7.35 (m, 3H), 7.30 (q, J = 6.9 Hz, 2H), 6.84 (s, 1H), 6.61 (d, J = 11.1 Hz, 2H), 4.33−4.25 (m, 1H), 4.24−4.12 (m, 4H), 3.96−3.88 (m, 2H), 3.36 (q, J = 6.3 Hz, 2H), 3.32−3.28 (m, 4H), 3.26−3.20 (m, 4H), 2.90−2.84 (m, 4H), 2.74 (t, J = 6.5 Hz, 2H), 2.56−2.52 (m, 2H), 2.29−2.17 (m, 6H), 2.08 (s, 3H), 1.93−1.79 (m, 1H), 1.78−1.66 (m, 1H), 1.65−1.58 (m, 1H), 1.57−1.45 (m, 3H), 1.39−1.20 (m, 3H). LRMS (ESI+) m/z calcd for $C_{70}H_{68}F_4N_8O_{17}S_2$ $[M + H]^+$: 1433.4, found: 1433.4.

*(7S,22S)-1-(6,8-Difluoro-7-hydroxy-2-oxo-2H-chromen-3-yl)-7-(5-((2,5-dioxopyrrolidin-1-yl)oxy)-5-oxopentanamido)-1,8,12,20-tetraoxo-22-((3-oxo-3-((3-oxo-3-(((5R)-3,9,10,11-tetramethoxy-6,7-dihydro-5H-dibenzo[a,c][7]annulen-5-yl)-amino)propyl)amino)propyl)carbamoyl)-16,17-dithia-2,9,13,21-tetraazapentacosan-25-oic Acid (**18**).* **16** (15 mg, 0.011mmol) was dissolved in diethylamine/DMF (1:4, 1 mL) and stirred for 1 h. After complete cleavage of the Fmoc protecting group confirmed by mass spectral analysis, the solvent was removed under reduced pressure. The crude material was dissolved in DMF, and disuccinimidyl glutarate (35 mg, 0.11 mmol) and DIEA (19 μL, 0.11 mmol) were added. The solution was stirred for 16 h, and solvents removed under reduced pressure. The crude material was purified by RP-HPLC and lyophilized to afford **18** as a light yellow solid (7 mg, 47% yield). ^{1}H NMR (500 MHz, DMSO-d_6) 12.07 (brs, 1H), 8.78 (d, J = 1.3 Hz, 1H), 8.58 (t, J = 5.8 Hz, 1H), 8.39 (d, J = 8.4 Hz, 1H), 8.10 (d, J = 8.1 Hz, 1H), 8.04 (t, J = 5.7 Hz, 1H), 7.99−7.83 (m, 4H), 7.75 (dd, J = 10.4, 2.0 Hz, 1H), 7.24 (d, J = 8.1 Hz, 1H), 6.86 (d, J = 8.5 Hz, 2H), 6.76 (s, 1H), 4.60−4.46 (m, 1H), 4.29−4.10 (m, 3H), 3.82 (s, 3H), 3.78 (s, 3H), 3.77 (s, 3H), 3.47 (s, 3H), 3.35−3.14 (m, 11H), 2.92−2.84 (m, 2H), 2.80 (s, 2H), 2.75 (t, J = 6.9 Hz, 2H), 2.67 (t, J = 7.5 Hz, 1H), 2.54 (s, 4H), 2.49−2.44 (m, 1H), 2.39−2.29 (m, 2H), 2.27−2.10 (m, 8H), 2.07−1.99 (m, 1H), 1.92−1.78 (m, 3H), 1.74−1.57 (m, 2H), 1.56−1.43 (m, 3H), 1.37−1.19 (m, 2H). ^{13}C NMR (126 MHz, DMSO-d_6) δ 173.9, 171.7, 171.1, 170.9, 170.4, 170.2, 170.2, 170.2, 170.1, 169.6, 168.7, 160.9, 159.6, 158.4, 158.1, 157.8, 152.1, 150.3, 147.1, 141.8, 140.5, 134.7, 130.5, 126.1, 124.3, 117.5, 116.5, 110.8, 108.1, 99.5, 60.5, 55.8, 54.9, 52.4, 51.9, 48.2, 40.4, 38.3, 37.9, 37.1, 35.4, 35.3, 35.3, 35.2, 35.1, 34.90, 33.8, 33.5, 31.7, 31.4, 30.1, 30.07, 29.6, 28.7, 27.5, 25.4, 22.9, 20.4. LRMS (ESI+) m/z calcd for $C_{63}H_{77}F_2N_9O_{21}S_2$ $[M + H]^+$: 1398.5, found: 1398.5.

*(7S,22S)-22-((3-((2-(4-(2,7-Difluoro-6-hydroxy-3-oxo-3H-xanthen-9-yl)-3-methylbenzamido)ethyl)amino)-3-oxopropyl)carbamoyl)-1-(6,8-difluoro-7-hydroxy-2-oxo-2H-chromen-3-yl)-7-(5-((2,5-dioxopyrrolidin-1-yl)oxy)-5-oxopentanamido)-1,8,12,20-tetraoxo-16,17-dithia-2,9,13,21-tetraazapentacosan-25-oic Acid (**19**).* **17** (6 mg, 0.004 mmol) was dissolved in diethylamine/DMF (1:4, 1 mL) and stirred for 1 h. After complete cleavage of the Fmoc protecting group confirmed by mass spectral analysis, the solvent was removed with a Biotage V-10 Touch. The crude material was dissolved in DMF (0.45 mL), and disuccinimidyl glutarate (14 mg, 0.04 mmol) and DIEA (7 μL, 0.04 mmol) were added. The solution was stirred for 16 h. The crude product was diluted with DMSO (0.45 mL), purified by RP-HPLC, and lyophilized to afford **19** as a yellow solid (4 mg, 67% yield). ^{1}H NMR (500 MHz, DMSO-d_6) δ 12.07 (brs, 1H), 8.77 (s, 1H), 8.67 (t, J = 6.3 Hz, 1H), 8.57 (t, J = 5.6 Hz, 1H), 8.11 (d, J = 8.1 Hz, 1H), 8.04 (q, J = 5.2 Hz, 2H), 7.98−7.86 (m, 4H), 7.74 (dd, J = 10.6, 2.1 Hz, 1H), 7.39 (d, J = 7.8 Hz, 1H), 6.85 (brs, 1H), 6.61 (d, J = 11.0 Hz, 2H), 4.25−4.12 (m, 2H), 3.33−3.15 (m, 12H), 2.88 (t, J = 7.3 Hz, 2H), 2.81 (d, J = 4.3 Hz, 4H), 2.77−2.72 (m, 2H), 2.71−2.64 (m, 1H), 2.59 (s, 2H), 2.54 (s, 2H), 2.40 (t, J = 7.3 Hz, 2H), 2.30−2.17 (m, 8H), 2.14 (t, J = 7.4 Hz, 1H), 2.08 (s, 3H), 1.89−1.77 (m, 2H), 1.74−1.65 (m, 2H), 1.52−1.45 (m, 2H), 1.31−1.21 (m, 3H). LRMS (ESI+) m/z calcd for $C_{64}H_{67}F_4N_9O_{20}S_2$ $[M + Na]^+$: 1422.4, found: 1422.4.

Biological Assays and Protocols. SKBR3 breast cancer cells (ATCC HTB-30) were cultured in complete media comprising DMEM Nutrient Mixture F-12 Ham (Sigma Aldrich, D8437) supplemented with fetal bovine serum (10%, Hyclone-characterized FBS, SH3039603), penicillin (100 units/mL, Sigma Aldrich P4333), and streptomycin (100 μg/mL, Sigma Aldrich P4333). MDA-MB-468 breast cancer cells (ATCC HTB-132, a kind gift of Dr. Liang Xu) were cultured in complete media comprising DMEM (Sigma Aldrich, D6429) supplemented with fetal bovine serum (10%, Hyclone-characterized FBS, SH3039603), penicillin (100 units/mL, Sigma Aldrich P4333), and streptomycin (100 μg/mL, Sigma Aldrich P4333). All cells were grown in T75 flasks (CytoOne CC7682-4875) and incubated at 37 °C with 5% CO_2.

DOI: 10.1021/acsomega.9b01585
ACS Omega 2019, 4, 12955−12968

Confocal Microscopy. Imaging was performed using an inverted Leica TCS SPE confocal laser-scanning microscope fitted with a Leica 63× oil-immersion objective. Fluorescent probes were excited with either a 405 or 488 nm solid-state laser, and emitted photons were collected from 425 to 500 or 500 to 600 nm. Unless otherwise noted, laser power and PMT gain settings were identical for all images acquired within a given experiment to allow accurate comparisons of cellular fluorescence.

Flow Cytometry. A Beckman Coulter Cytoflex S (B2-R0-V2-Y2) flow cytometer was used for cellular analysis. Cells were excited with 405 and/or 488 nm diode lasers, and emitted photons were collected through 450/45 BP (Pacific Blue), 525/40 BP (Pennsylvania Green), or 690/50 nm BP (PI) filters. FSC threshold was set to 500 000, flow speed was fast, mixing and backflush times were 5 s.

Fluorescence Spectroscopy. Fluorescence spectra were recorded using a PerkinElmer LS-55 fluorescence spectrometer. Samples were excited at 405 or 488 nm, and emission was recorded from 425 to 700 or 515 to 700 nm with a scan speed of 500 nm/min and slit width of 10 nm. Samples were analyzed in a SUPRASIL macro/semimicro cell (PerkinElmer, B0631132)

Labeling of Antibodies with NHS Esters. Trastuzumab, obtained from a hospital pharmacy, was provided as a lyophilized powder mixed 1:1 with stabilizers (α,α-trehalose dihydrate, *L*-histidine, and polysorbate 20). Human IgG was provided as a lyophilized powder without stabilizers (Sigma, I4506). Trastuzumab was reconstituted in sterile PBS (pH 7.4) and passed through a spin column packed with Sephadex G-25 to remove the stabilizers. Briefly, Sephadex G-25 resin (Superfine, Sigma, S5772) was suspended in PBS (pH 7.4). The resulting slurry (950 μL) was added to a minispin column (USA Scientific, 1415-0600) and centrifuged (16 000*g*, 20 s) to remove the buffer and pack the resin. The antibody solution (no more than 75 μL per column) was loaded onto the packed resin and centrifuged (16 000*g*, 30 s) to separate the protein from the stabilizers. The concentration of trastuzumab was determined by absorbance at 280 nm using a Nanodrop 1000 instrument (IgG $\varepsilon_{1\%\ (10\ mg/mL)}$ = 13.7 L g^{-1} cm^{-1}). The concentration was adjusted to 100 μM using sterile PBS. IgG was reconstituted in sterile PBS (pH 7.4) and the concentration determined and adjusted as described above.

To label antibodies with NHS esters, the IgG in PBS (100 μM, 25−300 μL) was aliquoted into a 1.5 mL microcentrifuge tube. $NaHCO_3$ (aq., 1 M) was added (2.5−30 μL) to achieve a final concentration of 0.1 M. NHS esters were added as concentrated (typically 10 mM) DMSO stock solutions to achieve 5- to 10-fold excess over the antibody concentration. Solutions were incubated in a Big Shot III Hybridization oven (0.5 h, 37 °C). To purify the conjugates, Sephadex G-25 resin was packed into columns, as described above. The antibody solution was loaded onto the packed resin (no more than 75 μL per column) and centrifuged (16 000*g*, 30 s) to separate the protein from unconjugated small molecules. This was done twice to ensure full removal of toxins and larger fluorophores; once was sufficient for small fluorophores. Conjugates used for toxicity assays or other 72 h assays were additionally sterilized by passage through Ultra-MC centrifugal filters (0.22 μm, Millipore, UFC30GV0S) by centrifugation (13 000*g*, 3 min).

After purification, the degree of labeling (DOL) of each conjugate was determined by absorbance spectroscopy. Absorbance values at 280 and 425 or 488 nm (IgG, 280 nm $\varepsilon_{1\%\ (10\ mg/mL)}$ = 13.7 L g^{-1} cm^{-1}, Pacific Blue, 425 nm ε = 29 500 M^{-1} cm^{-1}, Fluorescein, 490 nm ε = 70 000 M^{-1} cm^{-1}, Pennsylvania Green, 490 nm ε = 60 000 M^{-1} cm^{-1}) were measured with a Nanodrop 1000 Spectrophotometer to quantify the average number of molecules per antibody. From the absorbance of **18** at 280 nm (4:1 DMSO/PBS), CME contributes an additional 30% of the absorbance of PB at 280 nm, and the concentrations and DOL of **4** and **5** were corrected[64] to account for this contribution.

Visualization of Endosome Disruption by Confocal Microscopy. Cells were seeded in complete media into 8-well μ-slides (Ibidi, 80826, 100 000 cells/mL, 300 μL/well) and allowed to adhere overnight. Each well was washed once with media, and then the media was replaced with complete media (150 μL) containing vehicle control (0.1% DMSO), fluorescent conjugate, and/or EDP at the indicated concentration. The concentrations of all DMSO stock solutions were normalized using extinction coefficients and UV−vis spectroscopy. Cells were incubated for 24 h, washed once with media, and imaged by confocal microscopy.

Analysis of Cytotoxicity. SKBR3 and MDA-MB-468 cells were used to analyze the toxicity of antibody−toxin conjugates. Cells were plated in the appropriate complete media into CytoOne 96-well tissue culture plates (USA Scientific, CC7682-7596) at 50 000 cells/mL (200 μL/well) and incubated for 16 h. On the same day, IgG and trastuzumab (50 μL each) were labeled with **18** (10-fold excess), as described above, to yield **4** at 50 μM (DOL = 5.9) and **5** at 53 μM (DOL = 5.7). The next day, DMSO stock solutions of *N*-acetylcolchinol methyl ether (**7**, 1 mM, ε = 20 000 M^{-1} cm^{-1} at 262 nm in EtOH), Chol-EDP (**3**, 10 mM, ε = 20 970 M^{-1} cm^{-1} at 280 nm in 4:1 DMSO/PBS), and HS-iCME (**8**, 10 mM, ε for **7** was used) were prepared and standardized by absorbance using molar extinction coefficients. These compounds were serially diluted 1:3 to yield 1000× DMSO stock solutions (0.3−300 μM for **7**, 10−10 000 μM for **3** and **8**). These solutions were diluted 1:1000 into complete media to yield final concentrations of 0.3−300 nM for **7** and 10−10 000 nM for **3** and **8** (Final [DMSO] = 0.1%). Media was aspirated from each well and replaced with this treated media (150 μL) in triplicate. Antibody conjugates were serially diluted in the appropriate complete media to yield solutions ranging from 0.03 to 1000 nM. Each sample was split into two equal aliquots, yielding two sets of samples for each conjugate. Chol-EDP (**3**, from a 2 mM DMSO stock solution) was added to one set of each conjugate so cells could be co-treated with the antibody conjugate and Chol-EDP. Media was aspirated from each well and replaced with the treated media (150 μL) in triplicate. After incubation for 72 h, the media was aspirated from each well, and each well was washed with PBS (100 μL). Cells were trypsinized by addition of 50 μL of trypsin to each well and incubation at 37 °C for 10 min. Trypsin was quenched with media (150 μL) containing propidium iodide (PI, 3 μM from a 3 mM PBS stock solution, Thermo Fisher Scientific, P1304MP), and cells in each well were pipetted repeatedly to break up clumps. Plates were immediately analyzed using a Beckman Coulter Cytoflex S (B2-R0-V2-Y2) flow cytometer. Cells were collected for 20 s per well. Other settings are described under Flow Cytometry. Light scattering and staining with PI were used to identify populations of living cells. Counts of viable cells for each treatment, determined in triplicate, were used to generate dose−response curves. These curves were fitted by nonlinear regression with an inhibitor vs

DOI: 10.1021/acsomega.9b01585
ACS Omega 2019, 4, 12955−12968

response 3-parameter model (GraphPad Prism 8) to determine IC_{50} values.

Analysis of SKBR3 Cells Treated with 6 by Confocal Microscopy as a Function of Time. SKBR3 cells were plated in complete media onto 8-well μ-slides (Ibidi, 80826, 125 000 cells/mL, 300 μL/well) and allowed to adhere for 16 h. Each well was washed once with media. The media was replaced with complete media (100 μL) containing antibody conjugate **6** (1 μM) with or without **3** (2 μM). Additional controls shown in Figures S1 and S2 used cholesterylamine-SS-fluorescein[32] (250 nM) as a fluorescent probe to further confirm the endosome-disruptive activity of **3** in a given set of experiments. Cells were incubated at 4 °C for 0.5 h. Cells were washed twice with media (with the exception of cells treated with cholesterylamine-SS-fluorescein,[32] which diffuses away over time), and the media was replaced with media (300 μL), containing **3** (2 μM) where appropriate. Cells were immediately imaged as described in Confocal Microscopy for the t = 0 time point. Cells were incubated at 37 °C prior to imaging for all other time points.

Analysis of SKBR3 Cells Treated with 6 by Flow Cytometry as a Function of Time. SKBR3 cells were plated in complete media into CytoOne 96-well tissue culture plates (USA Scientific, CC7682-7596) at 75 000 cells/mL (200 μL/well) and incubated overnight (16 h). On the same day, trastuzumab (300 μL) was labeled with **19** (4-fold excess) as described above to yield **6** at 62 μM (DOL = 2.6). As a fully cleaved control, trastuzumab−PB−SH was prepared from **6** by the addition of DTT (1 mM) to **6** followed by incubation (37 °C) in a Big Shot III Hybridization Oven (2 h). Fluorescence emission was monitored, and the reaction was allowed to proceed until the fluorescence stopped increasing (Figure S6). The solution was purified using Sephadex G-25 and filter sterilized as described above to yield trastuzumab−PB−SH (58 μM, DOL = 2.0). Trastuzumab (75 μL each) was additionally labeled on lysines with only Pennsylvania Green NHS ester or Pacific Blue NHS ester (2-fold excess of each) to produce trastuzumab-PG (70 μM, DOL 1.5) and trastuzumab−PB (62 μM, DOL 1.7) as additional controls to assure spectral orthogonality in both confocal microscopy and flow cytometry experiments (data not shown).

The next day, sufficient antibody conjugate (1 μM) in media was prepared with and without **3** (2 μM) to dose wells in triplicate (100 μL) and obtain 8 time points. Media was also prepared with Cholesterylamine-SS-Fluorescein[32] (250 nM) with and without **3** (2 μM) as a positive control to confirm endosome disruption by **3** (data not shown). The media was aspirated from the wells and replaced with this treated media (100 μL) in triplicate. Cells were incubated at 4 °C for 0.5 h. Cells were then washed once with media, and the media was replaced with media (200 μL), containing **3** (2 μM) where appropriate. Wells corresponding to time point t = 0 were immediately trypsinized as described in Analysis of Cytotoxicity, with the exception that PI was not added. Cells were analyzed as described in Flow Cytometry. Cells were incubated at 37 °C until the next time point.

To determine the half-life of the release of the Pennsylvania Green derivative from **6**, median blue fluorescence values from each well were collected. The values of **6** with and without **3** were multiplied by 0.83 to correct for the lower efficacy of binding of trastuzumab−PB for HER2 after treatment with DTT compared to **6**. These values were divided by the corresponding values of trastuzumab−PB−SH (as a control for complete cleavage of **6**) with and without **3**. These ratios were then normalized using the value at t = 0 as representative of 0% cleavage and a ratio of one as representative of 100% cleavage. The half-life was determined by curve fitting using a one-phase association model (GraphPad Prism 8). The normalized ratios of each time point with and without **3** were compared using unpaired t tests (one per time point) with the assumption that all data were sampled from populations with the same scatter using the Holm−Sidak method (α = 5%). The differences in half-lives with and without **3** were not significant.

■ ASSOCIATED CONTENT

Supporting Information

The Supporting Information is available free of charge on the ACS Publications website at DOI: 10.1021/acsomega.9b01585.

Comparison of endosome disruptive activity of known and novel lipopeptides; additional confocal micrographs of treated SKBR3 and MDA-MB-468 cells; quantification of cellular fluorescence from antibody-iCME conjugates; cleavage of disulfides of antibody conjugates by DTT; colocalization of conjugate **6** with LysoTracker Red DND-99 in SKBR3 cells; methods, and compound characterization data (PDF)

Compounds **3** (Chol-EDP) and **8** (SH-iCME) (CSV)

■ AUTHOR INFORMATION

Corresponding Author

*E-mail: brpeters@ku.edu.

ORCID

Blake R. Peterson: 0000-0001-8251-3579

Present Addresses

[†]Department of Chemistry, Texas A&M University, College Station, Texas 77843, United States (Z.G.).

[‡]Novo Nordisk Research Center, Seattle, Washington 98109, United States (D.H.).

[§]Urologic Oncology Branch, National Cancer Institute, Bethesda, Maryland 20892, United States (M.M.L.).

Notes

The authors declare no competing financial interest.

■ ACKNOWLEDGMENTS

We thank the NIH (R01-CA211720 and P20-GM103638) for financial support. K.E.K. thanks the ACS for a MEDI predoctoral fellowship and was supported in part by a NIH Pharmaceutical Aspects of Biotechnology Training Grant (T32-GM008359). D.H. thanks the ACS for a MEDI predoctoral fellowship and was supported in part by a NIH Dynamic Aspects of Chemical Biology Training grant (T32-GM008545). We thank Prof. Liang Xu for the MDA-MB-468 cell line.

■ ABBREVIATIONS

ADC, antibody drug conjugate; HER2, human epidermal growth factor receptor 2; EDP, endosome-disruptive peptide; CME, colchinol methyl ether; iCME, cell-impermeable derivative of colchinol methyl ether; FRET, Förster resonance energy transfer; SPPS, solid-phase peptide synthesis; AIB, 2-aminoisobutyric acid; NHS, *N*-hydroxysuccinimide; DOL, degree of labeling; IgG, immunoglobin G; DTT, dithiothreitol; HPLC, high pressure liquid chromatography; TFA, trifluoro-

DOI: 10.1021/acsomega.9b01585
ACS Omega 2019, 4, 12955−12968

acetic acid; DMF, dimethylformamide; HATU, hexafluorophosphate azabenzotriazole tetramethyl uronium; DIEA, *N*,*N*-diisopropylethylamine; TIPS, triisopropylsilane; 2-CTC, 2-chlorotrityl resin; DMSO, dimethyl sulfoxide; TFE, trifluoroethanol; mPEG, 12-amino-4,7,10-trioxadodecanoic acid; EDC, 1-ethyl-3-(3-dimethylaminopropyl)carbodiimide; NMR, nuclear magnetic resonance; HRMS, high resolution mass spectroscopy; DAST, diethylaminosulfur trifluoride; PB, Pacific Blue fluorophore; PG, Pennsylvania Green fluorophore; PMT, photomultiplier tube; BP, bandpass filter; PBS, phosphate buffered saline (pH 7.4); ED, ethylenediamine

REFERENCES

(1) Beck, A.; Goetsch, L.; Dumontet, C.; Corvaia, N. Strategies and challenges for the next generation of antibody-drug conjugates. *Nat. Rev. Drug Discovery* **2017**, *16*, 315−337.

(2) Senter, P. D.; Sievers, E. L. The discovery and development of brentuximab vedotin for use in relapsed Hodgkin lymphoma and systemic anaplastic large cell lymphoma. *Nat. Biotechnol.* **2012**, *30*, 631−637.

(3) Lambert, J. M.; Chari, R. V. Ado-trastuzumab Emtansine (T-DM1): an antibody-drug conjugate (ADC) for HER2-positive breast cancer. *J. Med. Chem.* **2014**, *57*, 6949−6964.

(4) Bross, P. F.; Beitz, J.; Chen, G.; Chen, X. H.; Duffy, E.; Kieffer, L.; Roy, S.; Sridhara, R.; Rahman, A.; Williams, G.; Pazdur, R. Approval summary: gemtuzumab ozogamicin in relapsed acute myeloid leukemia. *Clin. Cancer Res.* **2001**, *7*, 1490−1496.

(5) Uy, N.; Nadeau, M.; Stahl, M.; Zeidan, A. M. Inotuzumab ozogamicin in the treatment of relapsed/refractory acute B cell lymphoblastic leukemia. *J. Blood Med.* **2018**, *9*, 67−74.

(6) Sapra, P.; Stein, R.; Pickett, J.; Qu, Z.; Govindan, S. V.; Cardillo, T. M.; Hansen, H. J.; Horak, I. D.; Griffiths, G. L.; Goldenberg, D. M. Anti-CD74 antibody-doxorubicin conjugate, IMMU-110, in a human multiple myeloma xenograft and in monkeys. *Clin. Cancer Res.* **2005**, *11*, 5257−5264.

(7) Lewis Phillips, G. D.; Li, G.; Dugger, D. L.; Crocker, L. M.; Parsons, K. L.; Mai, E.; Blattler, W. A.; Lambert, J. M.; Chari, R. V.; Lutz, R. J.; Wong, W. L.; Jacobson, F. S.; Koeppen, H.; Schwall, R. H.; Kenkare-Mitra, S. R.; Spencer, S. D.; Sliwkowski, M. X. Targeting HER2-positive breast cancer with trastuzumab-DM1, an antibody-cytotoxic drug conjugate. *Cancer Res.* **2008**, *68*, 9280−9290.

(8) Hamblett, K. J.; Kozlosky, C. J.; Siu, S.; Chang, W. S.; Liu, H.; Foltz, I. N.; Trueblood, E. S.; Meininger, D.; Arora, T.; Twomey, B.; Vonderfecht, S. L.; Chen, Q.; Hill, J. S.; Fanslow, W. C. AMG 595, an Anti-EGFRvIII Antibody-Drug Conjugate, Induces Potent Antitumor Activity against EGFRvIII-Expressing Glioblastoma. *Mol. Cancer Ther.* **2015**, *14*, 1614−1624.

(9) Oflazoglu, E.; Stone, I. J.; Gordon, K.; Wood, C. G.; Repasky, E. A.; Grewal, I. S.; Law, C. L.; Gerber, H. P. Potent anticarcinoma activity of the humanized anti-CD70 antibody h1F6 conjugated to the tubulin inhibitor auristatin via an uncleavable linker. *Clin. Cancer Res.* **2008**, *14*, 6171−6180.

(10) Kinneer, K.; Meekin, J.; Tiberghien, A. C.; Tai, Y. T.; Phipps, S.; Kiefer, C. M.; Rebelatto, M. C.; Dimasi, N.; Moriarty, A.; Papadopoulos, K. P.; Sridhar, S.; Gregson, S. J.; Wick, M. J.; Masterson, L.; Anderson, K. C.; Herbst, R.; Howard, P. W.; Tice, D. A. SLC46A3 as a Potential Predictive Biomarker for Antibody-Drug Conjugates Bearing Noncleavable Linked Maytansinoid and Pyrrolobenzodiazepine Warheads. *Clin. Cancer Res.* **2018**, *24*, 6570−6582.

(11) Scott, L. J. Brentuximab Vedotin: A Review in CD30-Positive Hodgkin Lymphoma. *Drugs* **2017**, *77*, 435−445.

(12) Dubowchik, G. M.; Firestone, R. A.; Padilla, L.; Willner, D.; Hofstead, S. J.; Mosure, K.; Knipe, J. O.; Lasch, S. J.; Trail, P. A. Cathepsin B-labile dipeptide linkers for lysosomal release of doxorubicin from internalizing immunoconjugates: model studies of enzymatic drug release and antigen-specific in vitro anticancer activity. *Bioconjugate Chem.* **2002**, *13*, 855−869.

(13) Rather, G. M.; Lin, S. Y.; Lin, H.; Banach-Petrosky, W.; Hirshfield, K. M.; Lin, C. Y.; Johnson, M. D.; Szekely, Z.; Bertino, J. R. Activated matriptase as a target to treat breast cancer with a drug conjugate. *Oncotarget* **2018**, *9*, 25983−25992.

(14) Kelly, R. K.; Olson, D. L.; Sun, Y.; Wen, D.; Wortham, K. A.; Antognetti, G.; Cheung, A. E.; Orozco, O. E.; Yang, L.; Bailly, V.; Sanicola, M. An antibody-cytotoxic conjugate, BIIB015, is a new targeted therapy for Cripto positive tumours. *Eur. J. Cancer* **2011**, *47*, 1736−1746.

(15) Younes, A.; Kim, S.; Romaguera, J.; Copeland, A.; Farial Sde, C.; Kwak, L. W.; Fayad, L.; Hagemeister, F.; Fanale, M.; Neelapu, S.; Lambert, J. M.; Morariu-Zamfir, R.; Payrard, S.; Gordon, L. I. Phase I multidose-escalation study of the anti-CD19 maytansinoid immunoconjugate SAR3419 administered by intravenous infusion every 3 weeks to patients with relapsed/refractory B-cell lymphoma. *J. Clin. Oncol.* **2012**, *30*, 2776−2782.

(16) Widdison, W.; Wilhelm, S.; Veale, K.; Costoplus, J.; Jones, G.; Audette, C.; Leece, B.; Bartle, L.; Kovtun, Y.; Chari, R. Metabolites of antibody-maytansinoid conjugates: characteristics and in vitro potencies. *Mol. Pharmaceutics* **2015**, *12*, 1762−1773.

(17) Kellogg, B. A.; Garrett, L.; Kovtun, Y.; Lai, K. C.; Leece, B.; Miller, M.; Payne, G.; Steeves, R.; Whiteman, K. R.; Widdison, W.; Xie, H.; Singh, R.; Chari, R. V.; Lambert, J. M.; Lutz, R. J. Disulfide-linked antibody-maytansinoid conjugates: optimization of in vivo activity by varying the steric hindrance at carbon atoms adjacent to the disulfide linkage. *Bioconjugate Chem.* **2011**, *22*, 717−727.

(18) Donaghy, H. Effects of antibody, drug and linker on the preclinical and clinical toxicities of antibody-drug conjugates. *mAbs* **2016**, *8*, 659−671.

(19) Polson, A. G.; Calemine-Fenaux, J.; Chan, P.; Chang, W.; Christensen, E.; Clark, S.; de Sauvage, F. J.; Eaton, D.; Elkins, K.; Elliott, J. M.; Frantz, G.; Fuji, R. N.; Gray, A.; Harden, K.; Ingle, G. S.; Kljavin, N. M.; Koeppen, H.; Nelson, C.; Prabhu, S.; Raab, H.; Ross, S.; Slaga, D. S.; Stephan, J. P.; Scales, S. J.; Spencer, S. D.; Vandlen, R.; Wranik, B.; Yu, S. F.; Zheng, B.; Ebens, A. Antibody-drug conjugates for the treatment of non-Hodgkin's lymphoma: target and linker-drug selection. *Cancer Res.* **2009**, *69*, 2358−2364.

(20) Li, F.; Emmerton, K. K.; Jonas, M.; Zhang, X.; Miyamoto, J. B.; Setter, J. R.; Nicholas, N. D.; Okeley, N. M.; Lyon, R. P.; Benjamin, D. R.; Law, C. L. Intracellular Released Payload Influences Potency and Bystander-Killing Effects of Antibody-Drug Conjugates in Preclinical Models. *Cancer Res.* **2016**, *76*, 2710−2719.

(21) Kratschmer, C.; Levy, M. Targeted Delivery of Auristatin-Modified Toxins to Pancreatic Cancer Using Aptamers. *Mol. Ther. Nucleic Acids* **2018**, *10*, 227−236.

(22) Rossin, R.; Versteegen, R. M.; Wu, J.; Khasanov, A.; Wessels, H. J.; Steenbergen, E. J.; Ten Hoeve, W.; Janssen, H. M.; van Onzen, A.; Hudson, P. J.; Robillard, M. S. Chemically triggered drug release from an antibody-drug conjugate leads to potent antitumour activity in mice. *Nat. Commun.* **2018**, *9*, No. 1484.

(23) Rossin, R.; van Duijnhoven, S. M.; Ten Hoeve, W.; Janssen, H. M.; Kleijn, L. H.; Hoeben, F. J.; Versteegen, R. M.; Robillard, M. S. Triggered Drug Release from an Antibody-Drug Conjugate Using Fast "Click-to-Release" Chemistry in Mice. *Bioconjugate Chem.* **2016**, *27*, 1697−1706.

(24) Nakase, I.; Kobayashi, S.; Futaki, S. Endosome-disruptive peptides for improving cytosolic delivery of bioactive macromolecules. *Biopolymers* **2010**, *94*, 763−770.

(25) Lonn, P.; Kacsinta, A. D.; Cui, X. S.; Hamil, A. S.; Kaulich, M.; Gogoi, K.; Dowdy, S. F. Enhancing Endosomal Escape for Intracellular Delivery of Macromolecular Biologic Therapeutics. *Sci. Rep.* **2016**, *6*, No. 32301.

(26) Steinauer, A.; LaRochelle, J. R.; Knox, S. L.; Wissner, R. F.; Berry, S.; Schepartz, A. HOPS-dependent endosomal fusion required for efficient cytosolic delivery of therapeutic peptides and small proteins. *Proc. Natl. Acad. Sci. U.S.A.* **2019**, *116*, 512−521.

(27) Su, X.; Fricke, J.; Kavanagh, D. G.; Irvine, D. J. In vitro and in vivo mRNA delivery using lipid-enveloped pH-responsive polymer nanoparticles. *Mol. Pharmaceutics* **2011**, *8*, 774−787.

DOI: 10.1021/acsomega.9b01585
ACS Omega 2019, 4, 12955−12968

(28) Ren, Y.; Hauert, S.; Lo, J. H.; Bhatia, S. N. Identification and characterization of receptor-specific peptides for siRNA delivery. *ACS Nano* **2012**, *6*, 8620−8631.
(29) Febvay, S.; Marini, D. M.; Belcher, A. M.; Clapham, D. E. Targeted cytosolic delivery of cell-impermeable compounds by nanoparticle-mediated, light-triggered endosome disruption. *Nano Lett.* **2010**, *10*, 2211−2219.
(30) Beaudoin, S.; Rondeau, A.; Martel, O.; Bonin, M. A.; van Lier, J. E.; Leyton, J. V. ChAcNLS, a Novel Modification to Antibody-Conjugates Permitting Target Cell-Specific Endosomal Escape, Localization to the Nucleus, and Enhanced Total Intracellular Accumulation. *Mol. Pharmaceutics* **2016**, *13*, 1915−1926.
(31) Su, X.; Yang, N.; Wittrup, K. D.; Irvine, D. J. Synergistic antitumor activity from two-stage delivery of targeted toxins and endosome-disrupting nanoparticles. *Biomacromolecules* **2013**, *14*, 1093−1102.
(32) Sun, Q.; Cai, S.; Peterson, B. R. Selective disruption of early/recycling endosomes: release of disulfide-linked cargo mediated by a N-alkyl-3beta-cholesterylamine-capped peptide. *J. Am. Chem. Soc.* **2008**, *130*, 10064−10065.
(33) Austin, C. D.; De Maziere, A. M.; Pisacane, P. I.; van Dijk, S. M.; Eigenbrot, C.; Sliwkowski, M. X.; Klumperman, J.; Scheller, R. H. Endocytosis and sorting of ErbB2 and the site of action of cancer therapeutics trastuzumab and geldanamycin. *Mol. Biol. Cell* **2004**, *15*, 5268−5282.
(34) Du, J.; Wang, H.; Zhong, C.; Peng, B.; Zhang, M.; Li, B.; Huo, S.; Guo, Y.; Ding, J. Structural basis for recognition of CD20 by therapeutic antibody Rituximab. *J. Biol. Chem.* **2007**, *282*, 15073−15080.
(35) Hirosue, S.; Weber, T. pH-Dependent lytic peptides discovered by phage display. *Biochemistry* **2006**, *45*, 6476−6487.
(36) Marshall, G. R.; Hodgkin, E. E.; Langs, D. A.; Smith, G. D.; Zabrocki, J.; Leplawy, M. T. Factors Governing Helical Preference of Peptides Containing Multiple Alpha,Alpha-Dialkyl Amino-Acids. *Proc. Natl. Acad. Sci. U.S.A.* **1990**, *87*, 487−491.
(37) Mitra, K.; Ubarretxena-Belandia, I.; Taguchi, T.; Warren, G.; Engelman, D. M. Modulation of the bilayer thickness of exocytic pathway membranes by membrane proteins rather than cholesterol. *Proc. Natl. Acad. Sci. U.S.A.* **2004**, *101*, 4083−4088.
(38) Sun, W.-C.; Gee, K. R.; Haugland, R. P. Synthesis of novel fluorinated coumarins: Excellent UV-light excitable fluorescent dyes. *Bioorg. Med. Chem. Lett.* **1998**, *8*, 3107−3110.
(39) Ravelli, R. B. G.; Gigant, B.; Curmi, P. A.; Jourdain, I.; Lachkar, S.; Sobel, A.; Knossow, M. Insight into tubulin regulation from a complex with colchicine and a stathmin-like domain. *Nature* **2004**, *428*, 198−202.
(40) Bagnato, J. D.; Eilers, A. L.; Horton, R. A.; Grissom, C. B. Synthesis and characterization of a cobalamin-colchicine conjugate as a novel tumor-targeted cytotoxin. *J. Org. Chem.* **2004**, *69*, 8987−8996.
(41) Ghawanmeh, A. A.; Chong, K. F.; Sarkar, S. M.; Bakar, M. A.; Othaman, R.; Khalid, R. M. Colchicine prodrugs and codrugs: Chemistry and bioactivities. *Eur. J. Med. Chem.* **2018**, *144*, 229−242.
(42) Brossi, A.; Sharma, P. N.; Atwell, L.; Jacobson, A. E.; Iorio, M. A.; Molinari, M.; Chignell, C. F. Biological effects of modified colchicines. 2. Evaluation of catecholic colchicines, colchifolines, colchicide, and novel N-acyl- and N-aroyldeacetylcolchicines. *J. Med. Chem.* **1983**, *26*, 1365−1369.
(43) Kang, G. J.; Getahun, Z.; Muzaffar, A.; Brossi, A.; Hamel, E. N-Acetylcolchinol O-Methyl Ether and Thiocolchicine, Potent Analogs of Colchicine Modified in the C-Ring - Evaluation of the Mechanistic Basis for Their Enhanced Biological Properties. *J. Biol. Chem.* **1990**, *265*, 10255−10259.
(44) Mottram, L. F.; Boonyarattanakalin, S.; Kovel, R. E.; Peterson, B. R. The Pennsylvania Green Fluorophore: A Hybrid of Oregon Green and Tokyo Green for the Construction of Hydrophobic and pH-Insensitive Molecular Probes. *Org. Lett.* **2006**, *8*, 581−584.
(45) Mottram, L. F.; Maddox, E.; Schwab, M.; Beaufils, F.; Peterson, B. R. A concise synthesis of the Pennsylvania Green fluorophore and labeling of intracellular targets with O6-benzylguanine derivatives. *Org. Lett.* **2007**, *9*, 3741−3744.
(46) Nicolaus, N.; Reball, J.; Sitnikov, N.; Velder, J.; Termath, A.; Fedorov, A. Y.; Schmalz, H. G. A Convenient Entry to New C-7-Modified Colchicinoids through Azide Alkyne [3+2] Cycloaddition: Application of Ring-Contractive Rearrangements. *Heterocycles* **2011**, *82*, 1585−1600.
(47) Besong, G.; Billen, D.; Dager, I.; Kocienski, P.; Sliwinski, E.; Tai, L. R.; Boyle, F. T. A synthesis of (aR,7S)-(-)-N-acetylcolchinol and its conjugate with a cyclic RGD peptide. *Tetrahedron* **2008**, *64*, 4700−4710.
(48) Hymel, D.; Cai, S.; Sun, Q.; Henkhaus, R. S.; Perera, C.; Peterson, B. R. Fluorescent mimics of cholesterol that rapidly bind surfaces of living mammalian cells. *Chem. Commun.* **2015**, *51*, 14624−14627.
(49) Rowland, C. E.; Brown, C. W.; Medintz, I. L.; Delehanty, J. B. Intracellular FRET-based probes: a review. *Methods Appl. Fluoresc.* **2015**, *3*, No. 042006.
(50) Zhang, H.; Liu, R.; Tan, Y.; Xie, W. H.; Lei, H.; Cheung, H. Y.; Sun, H. A FRET-based ratiometric fluorescent probe for nitroxyl detection in living cells. *ACS Appl. Mater. Interfaces* **2015**, *7*, 5438−5443.
(51) Lee, B. C.; Chalouni, C.; Doll, S.; Nalle, S. C.; Darwish, M.; Tsai, S. P.; Kozak, K. R.; Del-Rosario, G.; Yu, S. F.; Erickson, H.; Vandlen, R. FRET Reagent Reveals the Intracellular Processing of Peptide-Linked Antibody-Drug Conjugates. *Bioconjugate Chem.* **2018**, *29*, 2468−2477.
(52) Austin, M. A.; Hutter, C. M.; Zimmern, R. L.; Humphries, S. E. Genetic causes of monogenic heterozygous familial hypercholesterolemia: a HuGE prevalence review. *Am. J. Epidemiol.* **2004**, *160*, 407−420.
(53) Yang, J.; Chen, H.; Vlahov, I. R.; Cheng, J. X.; Low, P. S. Evaluation of disulfide reduction during receptor-mediated endocytosis by using FRET imaging. *Proc. Natl. Acad. Sci. U.S.A.* **2006**, *103*, 13872−13877.
(54) Erickson, H. K.; Lewis Phillips, G. D.; Leipold, D. D.; Provenzano, C. A.; Mai, E.; Johnson, H. A.; Gunter, B.; Audette, C. A.; Gupta, M.; Pinkas, J.; Tibbitts, J. The effect of different linkers on target cell catabolism and pharmacokinetics/pharmacodynamics of trastuzumab maytansinoid conjugates. *Mol. Cancer Ther.* **2012**, *11*, 1133−1142.
(55) Widdison, W. C.; Wilhelm, S. D.; Cavanagh, E. E.; Whiteman, K. R.; Leece, B. A.; Kovtun, Y.; Goldmacher, V. S.; Xie, H.; Steeves, R. M.; Lutz, R. J.; Zhao, R.; Wang, L.; Blattler, W. A.; Chari, R. V. Semisynthetic maytansine analogues for the targeted treatment of cancer. *J. Med. Chem.* **2006**, *49*, 4392−4408.
(56) Austin, C. D.; Wen, X.; Gazzard, L.; Nelson, C.; Scheller, R. H.; Scales, S. J. Oxidizing potential of endosomes and lysosomes limits intracellular cleavage of disulfide-based antibody-drug conjugates. *Proc. Natl. Acad. Sci. U.S.A.* **2005**, *102*, 17987−17992.
(57) Montero, D.; Tachibana, C.; Rahr Winther, J.; Appenzeller-Herzog, C. Intracellular glutathione pools are heterogeneously concentrated. *Redox Biol.* **2013**, *1*, 508−513.
(58) Phan, U. T.; Arunachalam, B.; Cresswell, P. Gamma-interferon-inducible lysosomal thiol reductase (GILT). Maturation, activity, and mechanism of action. *J. Biol. Chem.* **2000**, *275*, 25907−25914.
(59) Yu, X.; Liu, Q.; Wu, J.; Zhang, M.; Cao, X.; Zhang, S.; Wang, Q.; Chen, L.; Yi, T. Sonication-triggered instantaneous gel-to-gel transformation. *Chemistry* **2010**, *16*, 9099−9106.
(60) Lee, S. Y.; Liang, F.; Guo, X. L.; Xie, L. P.; Cahill, S. M.; Blumenstein, M.; Yang, H. Y.; Lawrence, D. S.; Zhang, Z. Y. Design, construction, and intracellular activation of an intramolecularly self-silenced signal transduction inhibitor. *Angew. Chem., Int. Ed.* **2005**, *44*, 4242−4244.
(61) Lee, M. M.; Peterson, B. R. Quantification of Small Molecule-Protein Interactions using FRET between Tryptophan and the Pacific Blue Fluorophore. *ACS Omega* **2016**, *1*, 1266−1276.
(62) Kaduk, C.; Wenschuh, H.; Beyermann, M.; Forner, K.; Carpino, L. A.; Bienert, M. Synthesis of Fmoc-amino acid fluorides

DOI: 10.1021/acsomega.9b01585
ACS Omega 2019, 4, 12955−12968

via DAST, an alternative fluorinating agent. *Lett. Pept. Sci.* **1996**, *2*, 285−288.
(63) Woydziak, Z. R.; Fu, L.; Peterson, B. R. Efficient and Scalable Synthesis of 4-Carboxy-Pennsylvania Green Methyl Ester: A Hydrophobic Building Block for Fluorescent Molecular Probes. *ChemInform* **2014**, *45*, 158−164.
(64) Bhattacharyya, S.; Wang, S.; Reinecke, D.; Kiser, W., Jr.; Kruger, R. A.; DeGrado, T. R. Synthesis and evaluation of near-infrared (NIR) dye-herceptin conjugates as photoacoustic computed tomography (PCT) probes for HER2 expression in breast cancer. *Bioconjugate Chem.* **2008**, *19*, 1186−1193.

DOI: 10.1021/acsomega.9b01585
ACS Omega 2019, 4, 12955−12968